iScience

CellPress
OPEN ACCESS

Article

MicroRNA-30e-5p has an Integrated Role in the Regulation of the Innate Immune Response during Virus Infection and Systemic Lupus Erythematosus

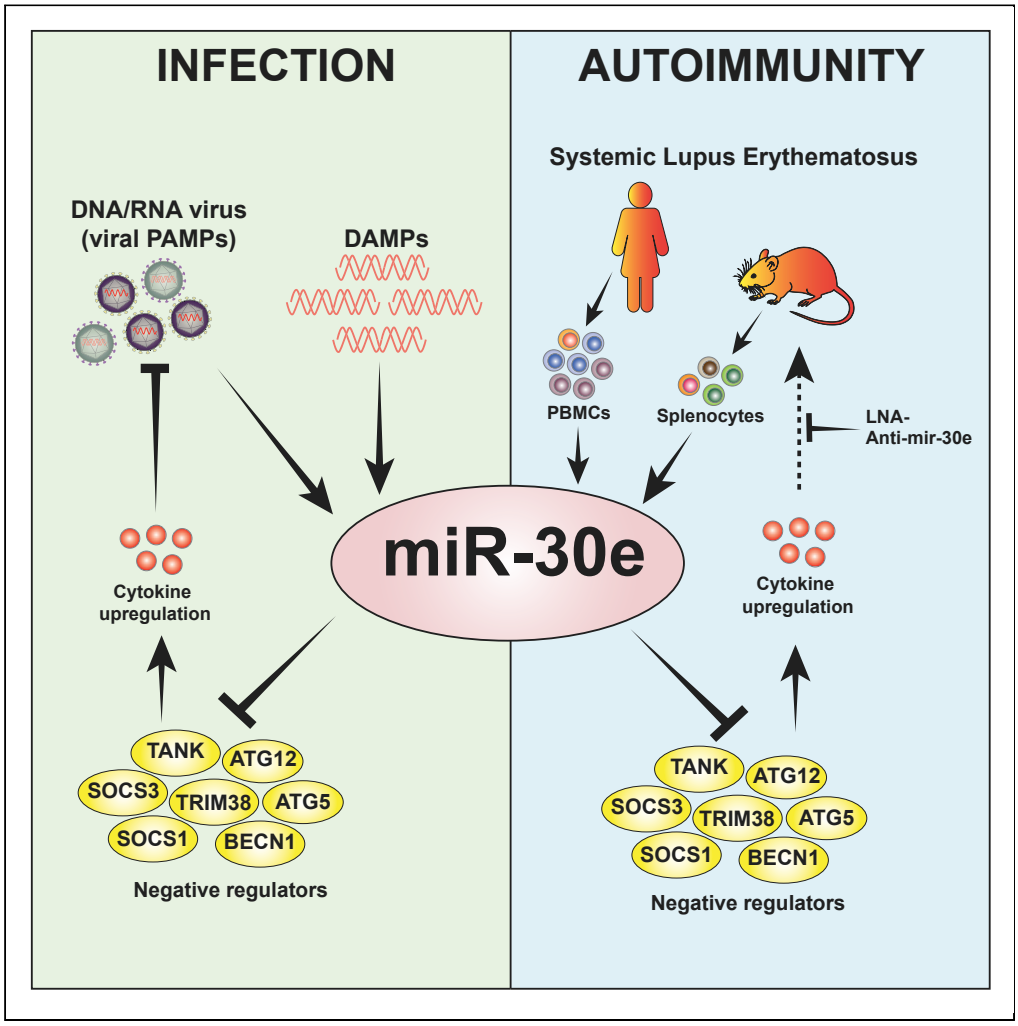

Richa Mishra, Sanjana Bhattacharya, Bhupendra Singh Rawat, ..., Prafullakumar Tailor, Akinori Takaoka, Himanshu Kumar

hkumar@iiserb.ac.in

HIGHLIGHTS

Pathogen (virus)/damage-associated molecular patterns induce microRNA-30e-5p

MiRNA-30e-5p regulates negative regulators of innate immune signaling pathways

Enhanced expression of miRNA-30e-5p may result in systemic lupus erythematosus (SLE)

Locked nucleic acid (LNA) inhibits miRNA-30e-5p and reduces molecular signatures of SLE

Mishra et al., iScience *23*, 101322
July 24, 2020
https://doi.org/10.1016/j.isci.2020.101322

iScience

CellPress
OPEN ACCESS

Article

MicroRNA-30e-5p has an Integrated Role in the Regulation of the Innate Immune Response during Virus Infection and Systemic Lupus Erythematosus

Richa Mishra,[1] Sanjana Bhattacharya,[1] Bhupendra Singh Rawat,[2] Ashish Kumar,[1] Akhilesh Kumar,[1] Kavita Niraj,[3] Ajit Chande,[4] Puneet Gandhi,[3] Dheeraj Khetan,[5] Amita Aggarwal,[6] Seiichi Sato,[7] Prafullakumar Tailor,[2] Akinori Takaoka,[7] and Himanshu Kumar[1,8,9,*]

SUMMARY

Precise regulation of innate immunity is crucial for development of appropriate host immunity against microbial infections and maintenance of immune homeostasis. MicroRNAs are small non-coding RNAs, post-transcriptional regulator of multiple genes, and act as a rheostat for protein expression. Here, we identified microRNA-30e-5p induced by hepatitis B virus and other viruses that act as a master regulator for innate immunity. Moreover, pegylated interferons treatment of patients with HBV for viral reduction also reduces miRNA. Additionally, we have also shown the immuno-pathological effects of miR-30e in patients with systemic lupus erythematosus (SLE) and mouse model. Mechanistically, miR-30e targets multiple negative regulators of innate immune signaling and enhances immune responses. Furthermore, sequestering of miR-30e in patients with SLE and mouse model significantly reduces type-I interferon and pro-inflammatory cytokines. Collectively, our study demonstrates the novel role of miR-30e in innate immunity and its prognostic and therapeutic potential in infectious and autoimmune diseases.

INTRODUCTION

Host innate immunity is an evolutionarily conserved defense system against microbial threats. These microbes express signature molecule known as pathogen-associated molecular patterns (PAMPs), which are sensed by host conserved sensors known as pattern-recognition receptors (PRRs) in various cellular compartments. The coordinated interactions among them activate a complex cascade of signaling pathways resulting in the development of innate immune responses, for the elimination of invading microbes, through production of pro-inflammatory cytokines, type I and III interferons (IFNs), chemokines, and recruitment of immune cells, and trigger cell death (Akira et al., 2006). These PRRs also sense host endogenous molecules known as damage/danger-associated molecular patterns (DAMPs) and trigger both heightened innate immune responses, including excesses interferon and cytokines production along with elevated TLRs activation, and cell death, resulting in the autoimmune disease, such lupus (Alvarez and Vasquez, 2017). These signatory features were reported to promote systemic lupus erythematous (SLE) (Yu et al., 2012; Devarapu and Anders, 2018). Elevated apoptosis and delay in clearance of apoptotic cellular bodies led to the accumulation of apoptotic debris, which is considered as a key process in the etiology of SLE, and it is also linked with the severity of SLE pathogenesis (Ronnblom and Leonard, 2019; Magna and Pisetsky, 2015; Mevorach, 2003; Munoz et al., 2008; Lovgren et al., 2004).

MicroRNAs (miRNAs) are a class of small non-coding RNAs (18–22 nucleotides) that fine-tune the protein expression through direct interaction with 3′ untranslated region (3′ UTR) of the gene transcript (He and Hannon, 2004). MicroRNA interacts with target transcript through base pairing and initiates degradation or blocking of translation machinery via multiprotein complex known as RNA-induced silencing complex (RISC) (Treiber et al., 2019). It has been reported that a single miRNA may have multiple mRNA targets and regulate cell signaling cascades and cellular responses during viral infections (Kim et al., 2015). Several viruses evade immune responses and establish infection by perturbing the host cellular miRNA expression or expressing viral(v)-miRNA upon infection (Zheng et al., 2013). In contrast, it has been reported that

[1]Laboratory of Immunology and Infectious Disease Biology, Department of Biological Sciences, Indian Institute of Science Education and Research (IISER) Bhopal, AB-3, Room No. 215, Bhopal By-pass Road, Bhauri, Bhopal, MP 462066, India

[2]Laboratory of Innate Immunity, National Institute of Immunology (NII), New Delhi 110067, India

[3]Department of Research (Medical Biotechnology), Bhopal Memorial Hospital & Research Centre (BMHRC), Bhopal, MP 462038, India

[4]Molecular Virology Laboratory, Department of Biological Sciences, Indian Institute of Science Education and Research (IISER) Bhopal, Bhopal, MP 462066, India

[5]Department of Transfusion Medicine, Sanjay Gandhi Postgraduate Institute of Medical Sciences (SGPGIMS), Lucknow, UP 226014, India

[6]Department of Clinical Immunology and Rheumatology, Sanjay Gandhi Postgraduate Institute of Medical Sciences (SGPGIMS), Lucknow, UP 226014, India

[7]Division of Signaling in Cancer and Immunology, Institute for Genetic Medicine, Hokkaido University, Sapporo, Japan

[8]WPI Immunology, Frontier Research Centre, Osaka University, Osaka 5650871, Japan

[9]Lead Contact

*Correspondence: hkumar@iiserb.ac.in

https://doi.org/10.1016/j.isci.2020.101322

several host miRNAs restrict viral replication by targeting viral genome or those host genes that are essential for viral replication (Ingle et al., 2015). In this study, we have hypothesized that the dysregulated microRNAs during virus infections might have strong implication on innate immune responses to counter the viral infection. Therefore, we identified miR-30e, induced by different DNA and RNA viruses in primary human cells and various mammalian cell lines, which restrict virus replication. Introduction of miR-30e into the cells enhances the innate immune responses and therefore reduces viral load. Notably, higher levels of miR-30e were also detected in the serum of therapy-naive patients with HBV and vice versa effects after pegylated type I IFNs treatment. We identified several negative regulators of PRR-mediated signaling pathways, such as *TRIM38*, *TANK*, *ATG5*, *ATG12*, *BECN1*, *SOCS1*, and *SOCS3*, that were targeted by miR-30e post-transcriptionally through RNA-induced silencing machinery (Porritt and Hertzog, 2015; Kondo et al., 2012). Additionally, we demonstrated that miR-30e plays a pivotal role in the reduction of transcripts of negative regulators through Argonaute 2 (AGO2) protein pull-down assay. The miR-30e enhances innate immune responses by targeting key negative regulators; therefore, we chose the systemic lupus erythematosus (SLE) model to understand the role of miR-30e under physiological condition. Previously, it has been shown that miR-30e level enhances in SLE, in the Korean population, although this was not characterized (Moulton et al., 2017; Shen et al., 2012; Kim et al., 2016). We observed that patients with SLE and SLE mouse model have shown higher expression of miR-30e. We also demonstrated an *ex vivo* introduction of miR-30e antagomir into PBMCs of patients with SLE and an *in vivo* intra-orbital injection of locked nucleic acid (LNA)-based inhibitor for miR-30e in SLE-induced mice that reduces type-I interferons and pro-inflammatory cytokines and moderately enhances the negative regulators. Altogether, our study demonstrates the novel role of miR-30e in innate immune regulation and its probable prognostic and therapeutic potential in virus infection and an autoimmune disorder, SLE.

RESULTS

Virus Infection Induces miRNA-30e to Inhibit Viral Infection through Enhancing Innate Antiviral Responses

To investigate the miRNAs involved in the regulation of innate immune response during viral infections, we performed unbiased data analyses on previously published reports and miRNA microarray GEO datasets as shown in the schematic workflow (Figure S1A). In particular, the miRNA reports in H5N1 (Vela et al., 2014) or Epstein-Barr virus (Gao et al., 2015) were analyzed for upregulated miRNAs. These upregulated miRNAs were compared with our previous miRNA profiling dataset from NDV infection in HEK293T cells (NCBI's Genbank_GSE65694). Upon comparison with NDV infection we selected miR-30e-5p, miR-27a-3p, and mir-181a/2-3p as the common miRNAs across miRNA profiles related to viral diseases (Figure S1B). Our analysis identified miR-30e as a unique miRNA that was predicted to target various PRR-mediated signaling regulators during negative regulation of innate immune responses (Figure S1C) and was upregulated in viral infections; moreover, its mature form was highly conserved among the wide range of species (Figure S1D). Additionally, datasets for H1N1 infection in mice (NCBI's Genbank_GSE69944), H5N1 infection in human lung carcinoma cells (A549 cells, NCBI's Genbank_GSE96857), and HBV-infected liver tissues of patients with hepatitis (NCBI's Genbank_GSE21279) were also analyzed by GEO2R package for upregulated miRNAs, and among all upregulated miRNAs, miR-30e upregulation is represented here (Figure S1E). The expression of miR-30e was upregulated during viral infections or stimulation with PAMPs *in vitro* in various cell lines (Figures S2A–S2F). At the transcriptional level, miR-30e promoter activity was moderately enhanced by NDV but was unaffected by *rh-IFNβ* or *rh-TNFα* stimulation, which activated the *ISRE*, *IFNβ*, and *NF-κB* promoters, respectively, suggesting that miR-30e expression might be induced by the viral infections but not by the cytokines produced during infection (Figures S2G–S2K).

To understand the clinical relevance, induction of miR-30e was tested in the cohort of 51 non-treated patients with HBV (demographic details mentioned in Table S1). Notably, the expression of miR-30e was evaluated from serum samples of therapy-naive patients with chronic hepatitis B (CHB) in comparison with healthy controls, and significant elevated levels of miR-30e were detected in patients with HBV (Figure 1A). Similar results were obtained with HepG2 cell line treated with serum from patients with HBV (HBV PS) for different time points; as shown (Figure 1B), the induction of miR-30e enhanced at 2 and 3 *dpi* (days post infection) with the highest expression at 3 *dpi*. Additionally, miR-30e mimic (miR-30e) inhibited HBV infection in HepG2 cells treated with serum from patients with HBV or in HepG2215 cells, stably expressing HBV replicon cells as compared with control miRNA (miR-NC1)-treated cells, which was tested by HBV-specific RNA and DNA quantification (Figures 1C and 1D) (Figure S3A). Interestingly, ectopic expression of miR-30e significantly reduced the HBV replication in HepG2-NTCP cells as tested by HBV RNA and HBV pgRNA

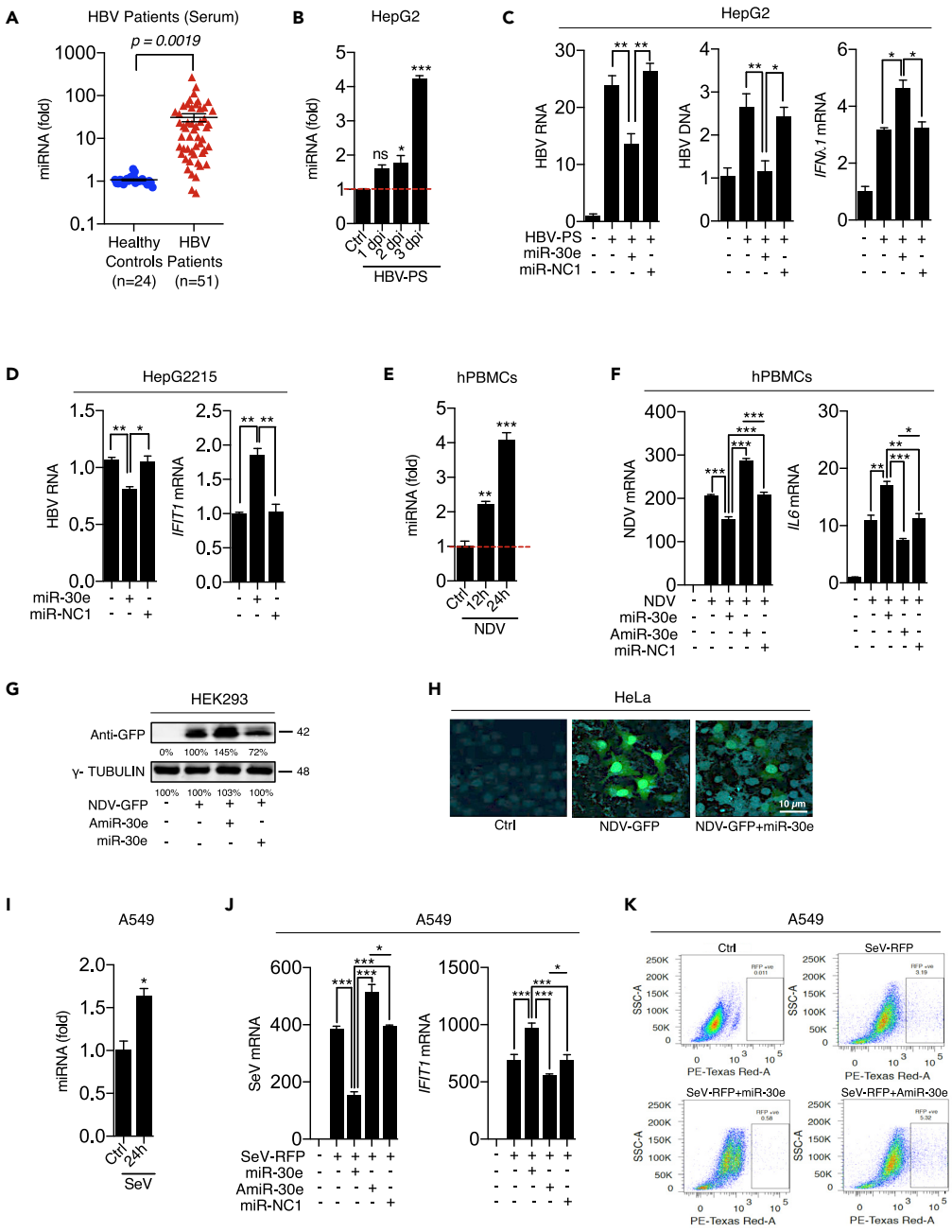

Figure 1. Viral Infection Induces miRNA-30e that Inhibits Virus Replication by Promoting Innate Immunity

(A) Quantification (as determined by qRT-PCR analysis) of the fold changes in the abundances of miR-30e as indicated, in the serum collected from patients with hepatitis B (n = 51) compared with healthy controls (n = 24).

(B–F, I, and J) Quantification of the fold changes in the relative abundances of miR-30e, viral transcripts, and respective innate immune transcripts (*IFNλ1*, *IL6*, and *IFIT1*) at the indicated times after treatment or infection with (B) HBV patient's serum (HBV PS) in HepG2 cells, (C) HepG2 cells were transfected with miR-30e (50 nM) or miR-NC1 (50 nM) prior to infection (D) HepG2215 cells, stably expressing HBV replicon HepG2 cells transfected with miR-30e or miR-NC1, (E) NDV (MOI 5) in human(H) PBMCs, (F) hPBMCs transfected with miR-30e or AmiR-30e (50 nM) or miR-NC1prior to infection, and (I) SeV (MOI 5) in A549 cells (J) A549 cells transfected with miR-30e or AmiR-30e or miR-NC1 prior to infection.

(G, H, and K) Quantification of viral infection as indicated in (G) HEK293 cells (transfected with miR-30e or AmiR-30e for 24 h then infected with GFP-tagged NDV (NDV-GFP) (MOI 5) for 36 h and subjected to immunoblot analysis using antibodies specific for GFP (anti-GFP antibody) and γ-tubulin (used as a loading control), (H) HeLa cells transfected with miR-30e or infected with NDV-GFP and subsequently subjected to confocal microscopic analysis for NDV particles

Figure 1. *Continued*

tagged with anti-GFP antibody (green), and nuclei were visualized with 4′,6-diamidino-2-phenylindole (DAPI; blue) and (K) A549 cells were transfected with miR-30e or AmiR-30e for 24 h then infected with RFP tagged SeV (MOI 5) for 24 h and analyzed by flow cytometry. Ctrl represents control untreated sample. Data are mean ± SEM of triplicate samples from single experiment and are representative of two (B–K) independent experiments. ***$p < 0.001$, **$p < 0.01$ and *$p < 0.05$ by one-way ANOVA Tukey test, Mann-Whitney test and unpaired t test. See also Figures S1–S6 and Table S1.

quantification (Figure S3B). Notably, we found significant elevated levels of HBV DNA and HBV covalently closed circular DNA in HBV patient serum infected HepG2 cells and stably expressing HBV replicon HepG2215 cells compared with uninfected HepG2 cells (Figures S3C and S3D) to show the infection status in the cells. On the other hand, expression of *IFNλ1* and *IFIT1* was enhanced in HepG2 and HepG2215 cells, respectively, in the presence of miR-30e (Figures 1C and 1D), and *IFNλ1* in HepG2215 cells (Figure S4A). Similarly, HBV infection in HepG2-NTCP cells (liver hepatoma cell line permissive for HBV infection through NTCP receptor) overexpressing miR-30e (ectopic) elevated *IFNλ1* transcript (Figure S4B). To study whether miR-30e was involved in controlling RNA virus infection, we infected human PBMCs (hPBMCs) with NDV to quantify the expression of miR-30e. We found that NDV infection elevated the expression of miR-30e in a time-dependent manner (Figure 1E). Additionally, PBMCs infected with NDV in the presence of miR-30e showed a significant reduction in NDV replication with a concomitant elevation of *IL6* expression compared with control (miR-NC1), whereas miR-30e inhibitor (AmiR-30e) reversed this phenomenon (Figure 1F). Similar inhibition of viral replication was observed in multiple cell lines infected with NDV in the presence of miR-30e or miR-NC1 (Figures S3E–S3G). Comparable results for antiviral responses were obtained after NDV infection in different cell types at the transcript and protein levels (Figures S4C–S4I) in the presence of miR-30e, and it also activated the *ISRE*, *IFNβ*, and *NF-κB* promoters as tested by luciferase assay (Figures S4J–S4L). Furthermore, miR-30e presence reduces NDV replication in terms NDV protein as tested by NDV-specific antibody estimated by western blot, microscopy, and FACS analysis, respectively (Figure 1G, 1H, and S3H). To further validate the function of miR-30e in controlling viral infections, we quantified the expression of miR-30e upon Sendai virus (SeV) infection in A549 cells. SeV induced the expression of miR-30e (Figure 1I), and ectopic expression of miR-30e (miR-30e mimic) inhibited the SeV replication as shown by qRT-PCR and FACS analysis (Figures 1J and 1K) through enhancing antiviral genes, such as the expression of *IFIT1* (Figure 1J).

Next, the role of miR-30e on DNA virus replication was determined; to this end, HFF cells were infected with DNA virus, HCMV, alone or along with miR-30e or miR-NC1. The viral replication was significantly reduced in the presence of miR-30e compared with the miR-NC1-treated HFF cells as quantified by HCMV transcript encoding viral glycoprotein gene (*Gly B*) by real-time PCR and analyzed by microscopy (Figure S5A), and additionally, the transcript levels of *IL6* was enhanced (Figure S5B).

To investigate how miR-30e influences antiviral responses upon treatment with pure viral ligand such as poly I:C and ssRNA, different cells including human PBMCs were transfected and stimulated, respectively, along with miR-30e.The expression of various ISGs and cytokines such as *IFNβ*, *CXCL10*, and *IL6* (Figures S6A–S6F) were elevated upon poly IC or ssRNA treatment along with miR-30e transfection, and similar results were found for the promoter activity of *ISRE* and *IFNβ* in the presence of miR-30e (Figures S6G and S6H). Collectively, our results demonstrate that miR-30e is upregulated during virus infection and miR-30e inhibits viral replication by promoting the expression of innate antiviral genes.

miR-30e Globally Enhances Innate Immune Responses during Virus Infection

To investigate the effect of miR-30e on innate immune responses upon virus infection, A549 cells were either mock transfected or transfected with miR-NC1 and miR-30e for 24 h, followed by infection with NDV for 24 h, and finally subjected to whole-transcriptome sequencing using an Illumina next-generation sequencer (NGS) and analyzed for differentially expressed genes as shown in the schematic (Figures 2A and S7A). Notably, the transfection efficiency of miR-30e in both replicates was confirmed by qRT-PCR using miR-30e-5p TaqMan assay and reduction in viral infection was confirmed by quantifying the NDV RNA in both the replicates to establish further analysis as per our previous findings (Figure 2B). Principal component analysis of the RNA-seq data for the samples resulted in the formation of three distinct groups (miR-30e, miR-NC1, and uninfected) according to their treatment (Figure 2C). Additional analysis of transcriptomic data showed that 1,179 genes were significantly upregulated and 1,206 genes were significantly downregulated upon miR-30e transfection in comparison with miR-NC1, represented by volcano plot

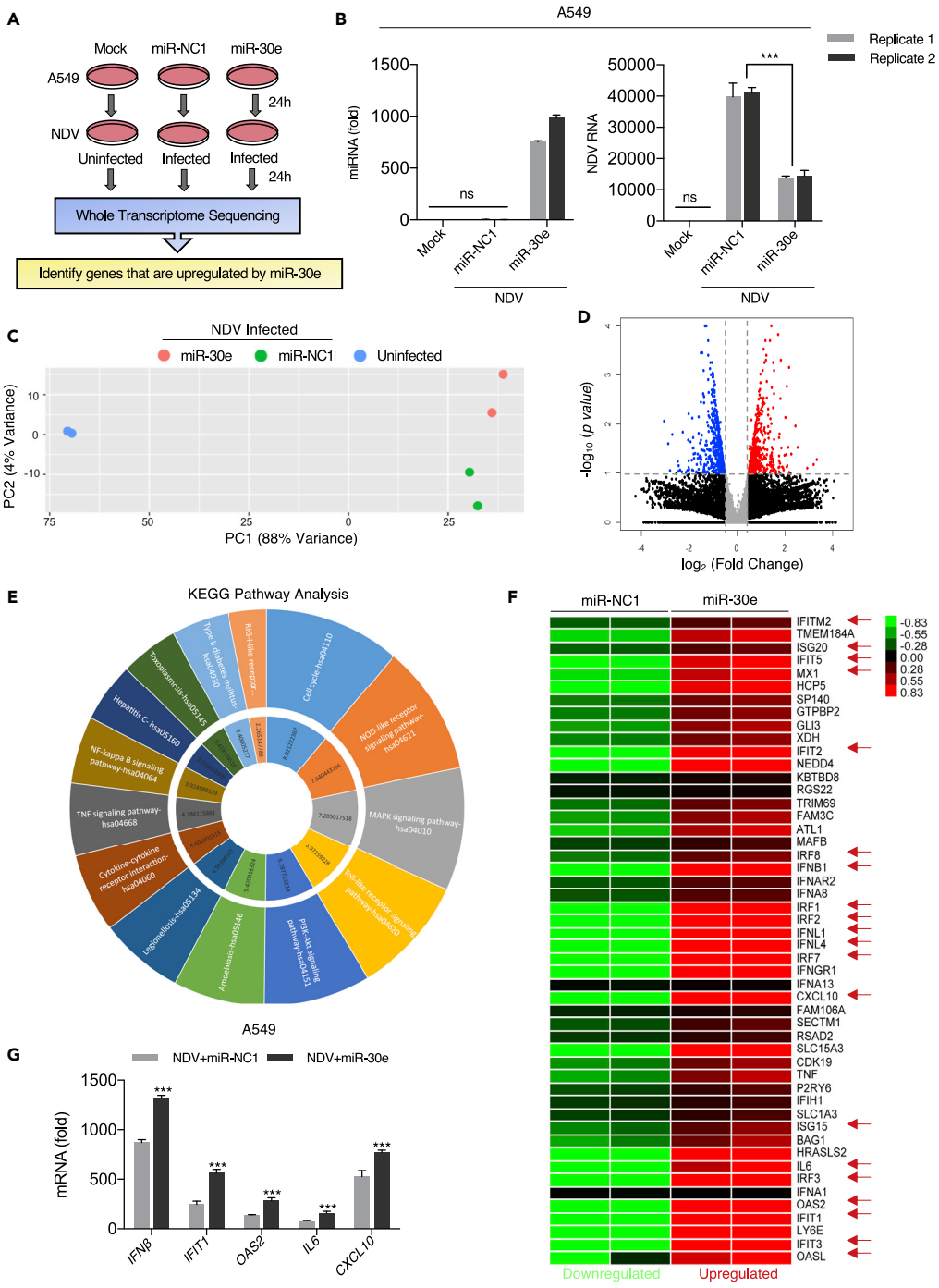

Figure 2. Transcriptomic Analysis Shows miR-30e Enhances Innate Immune Responses during NDV Infection

(A) Schematic outline of experimental setup, transfection with control (miR-NC1) or miR-30e and NDV infection (MOI 5) in A549 cells at indicated time, samples were subjected to whole-transcriptome sequencing and differential gene analysis.

(B) Quantification of the fold changes in the abundances of miR-30e is measured by qRT-PCR and normalized with U6 control, and NDV viral transcripts in both the replicate samples used for transcriptome sequencing and analysis.

(C) Plot showing first two components from principal component analysis of all the six samples, distance between samples indicate how different they are from each other in terms of gene expression.

(D) Volcano plot represents differential expression of genes between two groups of samples (miR-30e and miR-NC1 overexpression) during NDV infection in A549 cells. For each gene: *p value* is plotted against fold change (miR-30e vs miR-NC1). Genes significantly changed (>1.5-fold) are colored in red (upregulated) and blue (downregulated).

Figure 2. *Continued*

(E) KEGG pathway analysis of upregulated genes, outer circle indicates top upregulated pathways and the inner circle represents corresponding combined score (a derivative of *p value* and *Z* score).

(F) Heatmap represents the relative abundance of top upregulated interferon stimulated genes across different samples. Green color indicates downregulation and red color indicates upregulation of genes.

(G) Validation and quantification (measured by qRT-PCR) of the fold changes in the abundances of type 1 interferon and pro-inflammatory cytokines in the samples of A549 cells transfected with miR-NC1 or miR-30e and infected with NDV as indicated (NDV + miR-NC1) and (NDV + miR-30e), analyzed by RNA sequencing.

See also Figure S7.

(Figure 2D) and represented by MA plot (Bland-Altman plot where "M" represents log ratio and "A" represents mean average as plotting on MA scales) (Figure S7B). Moreover, KEGG pathway analysis of significantly upregulated genes, upon miR-30e treatment and NDV infection, indicated enrichment of genes belonging to key cellular machineries, namely, cell cycle, NOD-like receptor signaling pathway, MAPK signaling pathway, TLR signaling pathway, RLR signaling pathway, PI3K-AKT signaling pathway, cytokine-cytokine receptor interaction pathway, NF-κB signaling pathways, and TNF signaling pathway (Figure 2E). The relative expression levels of the highest expressing genes involved in these pathways is represented by heatmap (Figure S7C). Intriguingly, we noticed that a significant number of interferons-stimulated genes (ISGs) like *IFITM2*, *ISG20*, *IFIT5*, *MX1*, *IFIT2*, *IRF8*, *IFNB1*, *IRF1*, *IRF2*, *IFNL1*, *IFNL4*, *IRF7*, *CXCL10 (IP10)*, *ISG15*, *IL6*, *IRF3*, *OAS2*, *IFIT1*, *IFIT3*, and *OASL* were also predominantly upregulated (Figure 2F), which combines with the initial findings of the study. Furthermore, our NGS results were verified by quantifying the expression level of type 1 interferon *IFNβ*, interferon stimulated genes *IFIT1* and *OAS2*, and pro-inflammatory cytokines *IL6* and *CXCL10* (Figure 2G). These outcomes strongly suggest that miR-30e reduces the viral replication by enhancing the innate immune responses upon activation of various signaling cascades. Additionally, miR-30e impact on innate immune responses during viral infection prompted us to investigate transcriptome and gain mechanistic insight for the target of miR-30e.

miR-30e Targets Negative Regulators of PRR-Sensing and Interferon Signaling Pathways

To investigate the underlying molecular mechanism for the reduction of viral burden and enhanced antiviral innate immune responses by miR-30e, we conducted unbiased rigorous screening using various bioinformatic tools for the identification of innate immune genes. To filter the genes transcript targeted by miRNA, certain criterion for screening were applied. First of all, common genes involved in innate immune regulation upon viral infections and targeted by miR-30e were identified and subjected to KEGG pathway analysis. The analysis revealed that a majority of genes (*TRIM38*, *TANK*, *ATG5*, *ATG12*, *BECN1*, *SOCS1*, *SOCS3*, *TRIM13* and *EPG5*) were involved in negative/down regulation of PRRs-mediated signaling pathways (Figure 3A). Additionally, our NGS analysis demonstrated that expression of identified negative regulators during NDV infection were reduced upon miR-30e treatment as compared with the miR-NC1 group (Figure 3B). This further concludes that the negative regulators are the potential targets of mir-30e. The binding efficiency for miR-30e and identified targets genes are significantly high to alter any physiological functions by the miRNA that was tested by different *in silico* tools such as miRanda, DIANA, Target Scan, miRDB, and BiBiServ2_RNAhybrid as reported (Table S2). Although few targets of miR-30e are not negative regulators, the binding energy for those target transcript and miRNA assembly is low (Figure S8) and, therefore, it may not significantly alter the cellular function. To test the specificity of miRNA with the 3′ UTR of identified negative regulator genes, the 3′ UTR of the gene was cloned downstream of luciferase gene under the CMV promoter to perform the luciferase assay. It was found that miR-30e significantly reduced the luciferase activity of investigated genes compared with control miR-NC1 (Figure 3C). In contrast, introduction of mutation (3′ UTR_MUT) in cloned 3′ UTR/3′ UTR_WT by site-directed mutagenesis did not change the luciferase activity in the presence of miR-30e and it was comparable with 3′ UTR_WT (wild-type). miR-NC1 was used as a control for the experiment (Figure S9A); moreover, it could be noted here that the target sequence in each negative regulator genes was the same. Additionally, we knocked down these negative regulators in HEK-293T cells and infected them with NDV to further estimate the level of *IFNβ*, which clearly elucidated their inhibitory effect on the mRNA levels of *IFNβ* within a cell; this effect was found to be significant with respect to the majority of the targets (Figure 3D). And we observed that the production of *IFNβ* is comparable after knockdown of target genes and introduction of miR-30e into the cells during viral infection suggesting the pivotal role of miR-30e in the suppression of negative regulators transcripts. Furthermore, we scanned the 3′ UTRs of identified negative regulators for RNA-binding site for AGO2 protein, in CLIP database, which is a key component of the miRNA-mediated silencing complex (RISC) and found that the miR-30e strongly complexes with the target genes as shown in (Table S3). To validate miR-30e and

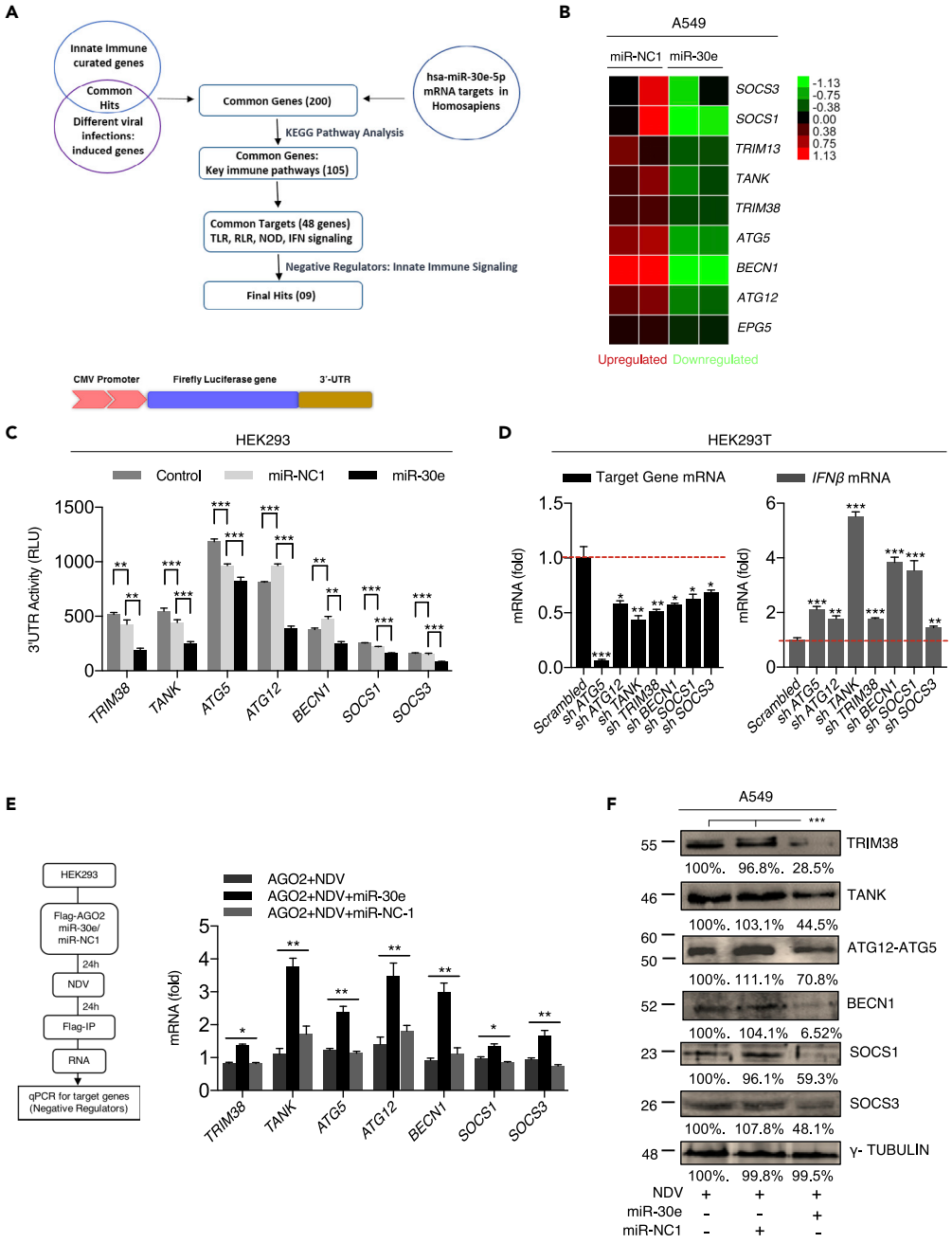

Figure 3. miR-30e Targets 3′ UTR of Negative Regulators of Innate Immune Signaling Pathways

(A) Screening pipeline used for identification of miR-30e target genes, based on the indicated schematic workflow, final hits of 09 genes corresponds to negative regulators targeted by miRNA-30e.

(B) RNA-seq analysis of transcriptome data for the identification of negative regulators (targeted by miR-30e) upon miR-30e transfection and NDV infection (MOI 5) compared with miR-NC1 in two replicate samples.

(C) HEK293 cells were transfected with 50 ng of pRL-TK and 300 ng of 3′ UTR_WT (of indicated genes) together with 25 nM miR-30e or miR-NC1 mimics; 24 h after transfection, the cell was lysed and subjected to luciferase assay.

(D) HEK293T cells were transiently transfected with 1.5 μg of *sh*-clones of indicated genes or scrambled control for 48 h then infected with NDV (MOI 5) for 24 h and subjected to the quantification of the indicated transcripts or genes and *IFNβ*.

(E) Schematic for RNA immunoprecipitation assay. HEK293 cells were transfected with plasmid encoding FLAG-AGO2 in presence of miR-30e (50 nM) and miR-NC1 (50 nM) and then infected with NDV (MOI 5). Twenty-four hours after transfection cells were subjected to RNA immunoprecipitation with anti-FLAG antibody and quantified for *TRIM38*, *TANK*, *ATG5*, *ATG12*, *BECN1*, *SOCS1*, and *SOCS3* transcripts.

Figure 3. *Continued*

(F) A549 cells were transfected with miR-30e or miR-NC1 mimic and then infected with NDV (MOI 5) for 36 h before being subjected to immunoblot analysis with antibodies specific for indicated protein or γ-tubulin (used as a loading control). Percentage represents the area under the curve/peak and/or intensity of the bands calculated by densitometry analysis using ImageJ software. Difference in the percentage of density between the three groups is statistically significant (performed using unpaired t test).

Data are mean ± SEM of triplicate samples from single experiment and are representative of three (C) and two (D–F) independent experiments. ***$p < 0.001$, **$p < 0.01$, and *$p < 0.05$ by one-way ANOVA Tukey test and unpaired t test. See also Figures S8–S10 and Tables S2 and S3.

negative regulator transcripts (*TRIM38*, *TANK*, *ATG5*, *ATG12*, *BECN1*, *SOCS1*, and *SOCS3*) interaction, AGO2 pull-down assay was performed as shown in schematic diagram (Figure 3E), and we found that introduction of miR-30e significantly enriches the transcript of negative regulators compared with the NDV alone infection or NDV infection along with control miR-NC1 treated cells suggesting that miRNA-30e directly interacts with the transcript through the formation of RISC.

Next, the ectopic expression of miR-30e reduced the expression level of these targets (*TRIM38*, *TANK*, *ATG5*, *ATG12*, *BECN1*, *SOCS1*, and *SOCS3*) in A549 cells compared with the control after NDV infection (Figure S9B). Consistent with these results induction of targets was also reduced in HBV-patient serum-treated HepG2 cells, HepG2215 cells stably expressing HBV replicon cells, and HepG2-NTCP cells infected with HBV, in the presence of miR-30e compared with the control miRNA transfection (Figures S10A–S10C), suggesting that miR-30e targets these genes during HBV and NDV infection in HepG2, HepG2215, HepG2-NTCP, and A549 cells, respectively. Similar results were obtained due to miR-30e transfection in NDV-infected and poly I:C-treated HeLa cells (Figures S10D and S10E). We not only confirmed the expression of negative regulators by analyzing transcripts but also tested for protein expression using specific antibodies by western blot analysis. The introduction of miR-30e significantly reduced the expression of *TRIM38*, *TANK*, *ATG12*, *BECN1*, *SOCS3*, and *SOCS1* as shown (Figure 3F). Therefore, our results strongly suggest that these key negative regulators of innate immunity are targeted by miR-30e, which are induced during virus infection and resulted in enhanced antiviral responses.

dsDNA (DAMP) Induces miR-30e and Enhances Innate Immune Responses

Our observation for induction of miR-30e and subsequent heightened innate immune responses upon viral infection or pure PAMPs stimulation prompted us to investigate the ability of host DAMPs for induction of miR-30e because sustained DAMPs production in the host can lead to enhanced sterile inflammation and subsequently it might establish autoimmune disease (Alvarez and Vasquez, 2017). To this end, *ex vivo* experiment was performed using hPBMCs from three healthy volunteers. The genomic DNA was extracted from a portion of hPBMCs and sonicated to make small fragments (approximately 110–150 bps) for efficient transfection into the cells (Figure 4A). The cultured hPBMCs were stimulated with the extracted small DNA fragments and tested for the induction of miR-30e and innate immune cytokines. The dsDNA (DAMP) stimulation significantly induces the miR-30e (Figure 4B) and expression of *IFNα*, *IFNβ*, *IFIT1*, and *IL6* genes in the cells of all three healthy volunteers (Figures 4C–4E). Next, to understand physiological significance of DAMP-induced innate immune cytokines, the dsDNA (DAMP)-stimulated cells were infected by NDV and NDV replication was measured. The dsDNA stimulation significantly reduced the NDV replication (Figure 4F) suggesting that inflammatory cytokines and type I interferons induced by dsDNA inhibited the viral replication, although inhibition of viral replication could be the collective result of both dsDNA and virus-mediated induction of proinflammatory cytokines, type I interferons, and type I inducible genes. Finally, we examined the levels of apoptosis induced by autologous dsDNA in hPBMCs by Annexin-PI assay using FACS analysis as shown in Figure S11A; dsDNA stimulation enhanced apoptosis compared with the mock stimulation, and it is comparable with the positive control treated cells, by Camptothecin. Additionally, the levels of *TLRs 3/7/9* were estimated upon dsDNA treatment as previously it has been reported that DAMPs enhance the levels of these *TLRs*. Consistent with previous observation, we obtained similar results (Figures S11B–S11D). Taken together, these results showed that DAMPs, particularly dsDNA, enhance miR-30e and innate immune responses as well as promote apoptosis and induce TLRs; these important characteristic features for the development of autoimmune disorder in co-occurrence with DAMPs (dsDNA) and miR-30e might play a pivotal role in autoimmune diseases.

Ex Vivo and *In Vivo* Dissemination of miR-30e

To investigate the role of miR-30e under physiological condition, an autoimmune disease, SLE, was selected because patients with SLE show enhanced inflammatory cytokines, type I interferons, and type I

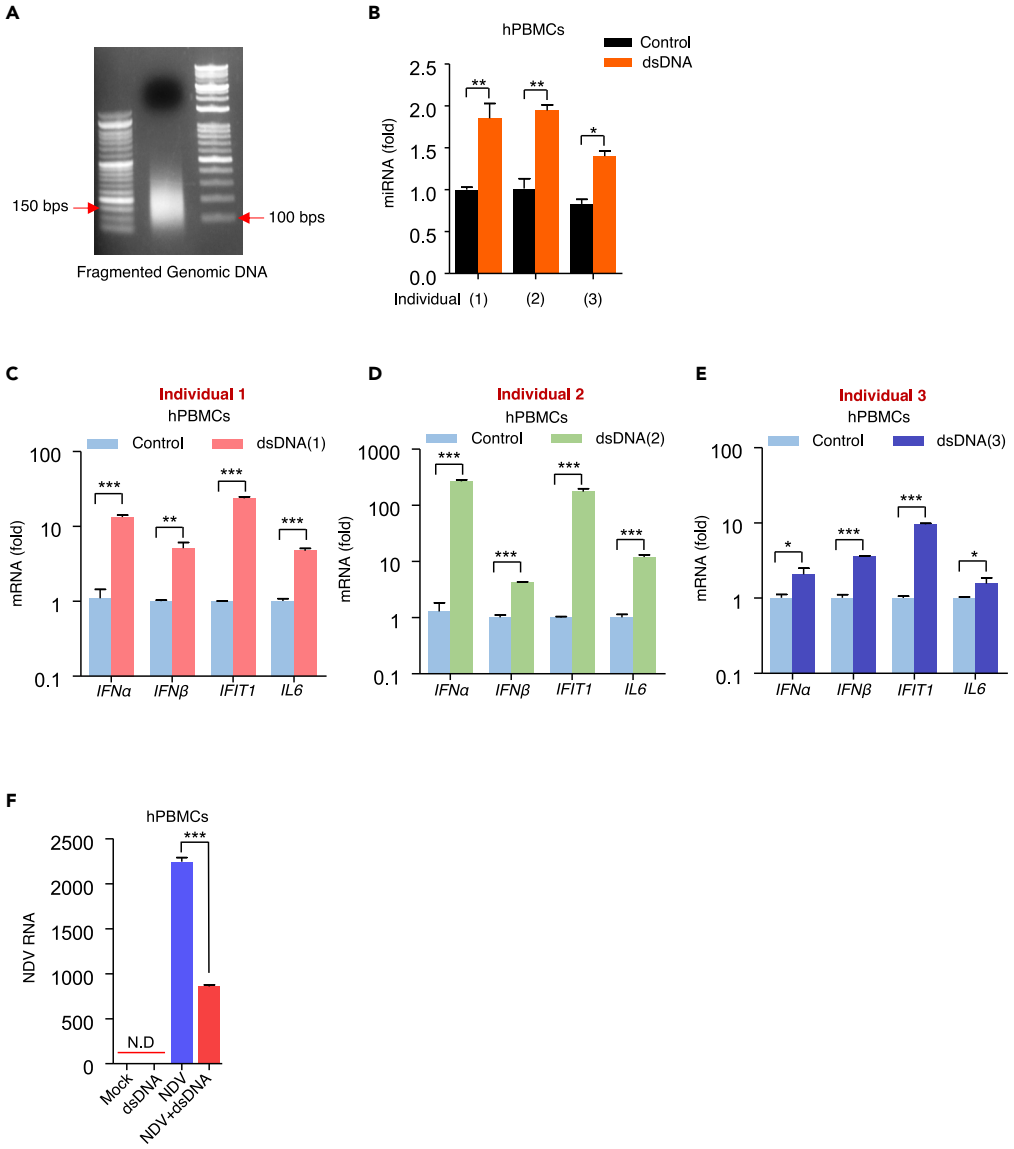

Figure 4. Human PBMCs Stimulated with dsDNA (DAMP) Induces miRNA-30e and Enhances Innate Immune Responses

PBMCs from three healthy individuals were transfected with their own genomic DNA (ds DNA).

(A) Isolated genomic DNA sonicated into small fragments of dsDNA of approximately 100–150 bps each (as shown) and transfected using Lipofectamine 2000.

(B–F) Quantification (by qRT-PCR analysis) of the fold changes in the relative abundances of (B) miR-30e, (C–E) respective innate immune transcripts (*IFNα*, *IFNβ*, *IFIT1*, and *IL6*) in all three individuals, and (F) NDV viral transcripts in presence of dsDNA.

Data are mean ± SEM of triplicate samples from single experiment and are representative of three independent experiments in three different individuals. ***p < 0.001, **p < 0.01, and *p < 0.05 by one-way ANOVA Tukey test and unpaired t test; N.D., not detected. See also Figure S11.

interferon-inducible cytokines production (Moulton et al., 2017). Patients with SLE also had elevated levels of several autoantibodies particularly antinuclear and anti-dsDNA antibodies. Therefore, PBMCs were isolated from clinically verified patients with SLE (P:n = 13) as shown (Table S4) and healthy controls (HC:n = 13) and cultured for 72 h, as shown in the schematic workflow (Figure 5A). The expression levels of *IFNβ*, *IFIT1*, and *IL6* were compared and quantified by qRT-PCR. As expected, we found that the expression levels of *IFNβ*, *IFIT1*, and *IL6* were significantly enhanced in patients with SLE compared with healthy controls

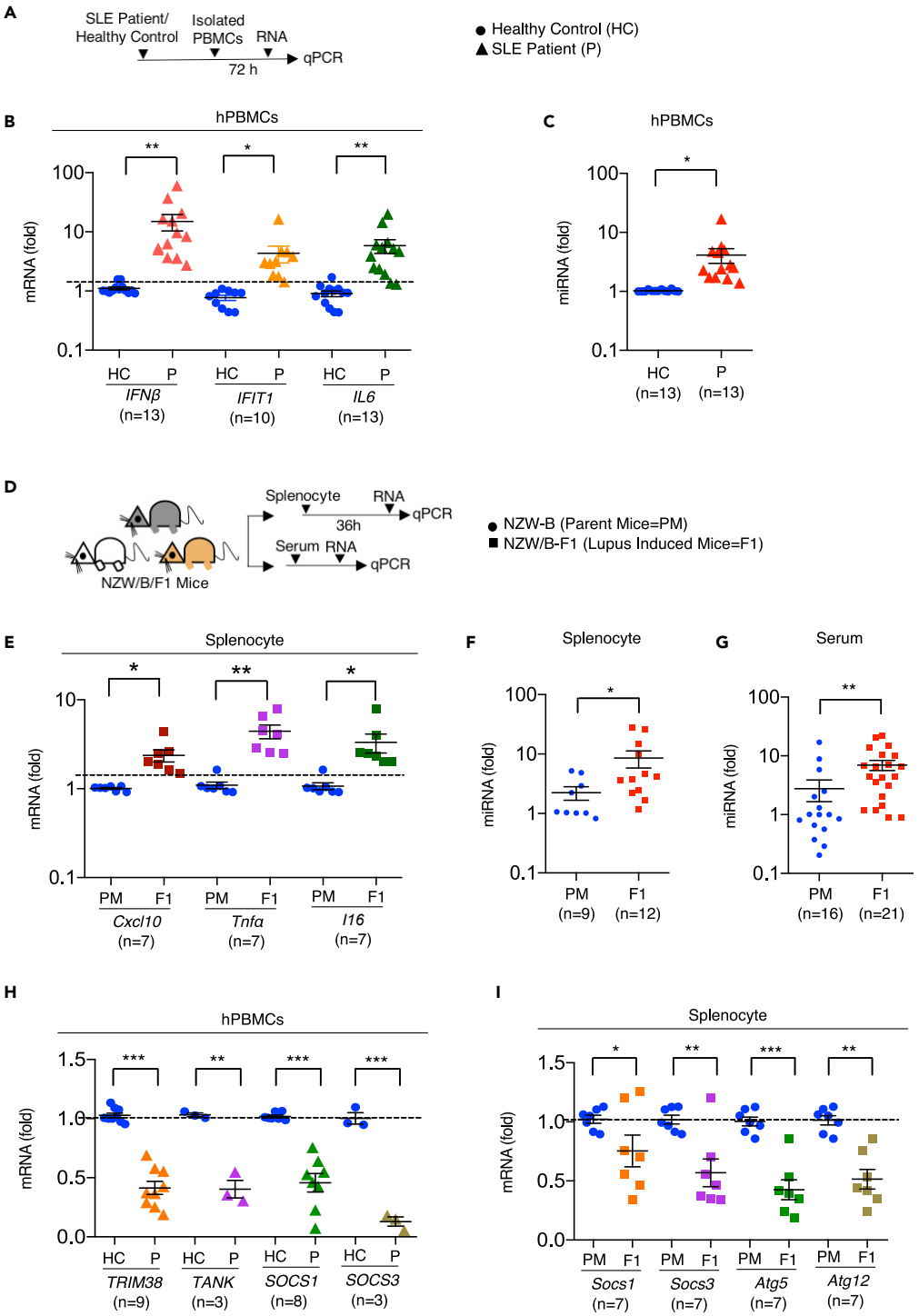

Figure 5. Enhanced Innate Immune Responses and miRNA-30e Expression Suppress Negative Regulators in the Patients with SLE and SLE Mouse Model

(A and D) Schematic representation of the workflow for quantification of relative expression by qRT-PCR analysis of indicated transcripts *IFNβ*, *IFIT1*,*IL6*, *TRIM38*, *TANK*, *SOCS1*, and *SOCS3* (in patients with SLE) and *Cxcl10*, *Tnfα*, *Il6*, *Socs1*, *Socs3*, *Atg5*, and *Atg12* (in SLE mice) and miR-30e at indicated time points in (B and C) PBMCs from SLE diagnosed patients (P) (n = 13) and healthy controls (HC) (n = 13). (E) Splenocytes from parent (New Zealand White and Black-NZW

Figure 5. *Continued*

and NZB) (PM) (n = 7) and lupus induced mice (NZW/B -F1 progeny) (F1) (n = 7) and (F and G) Splenocytes from PM (n = 9) and F1 (n = 12) and serum from PM (n = 16) and F1 (n = 21). Data are mean ± SEM of triplicate samples from single experiment and are representative of single (B, C and H) two independent experiments (E–G and I). ***p < 0.001, **p < 0.01, and *p < 0.05 by unpaired t test Mann-Whitney test. See also Figures S12 and S13 and Table S4.

(Figure 5B). The enhanced innate immune responses prompted us to investigate the expression levels of miR-30e. Interestingly, the expression of miR-30e is significantly enhanced (several fold) in patients (n = 13) compared with healthy controls (n = 13) (Figure 5C). Further to confirm our observations in patients with SLE, the SLE mouse model was used. The New Zealand white/black (NZW/B) mice were extensively used for SLE studies as shown in the schematic workflow (Figure 5D). The splenocytes from both parents NZB and/or NZW mice (n = 7) mice and lupus prone F1 (F1: NZW/B n = 7) generation mice were tested for the expression levels of *Cxcl10*, *Tnfα*, and *Il6* by qRT-PCR (Figure 5E). The F1 mice showed a significantly high level of inflammatory responses compared with non-SLE parent mice. Consistent with human SLE results, the expression of miR-30e is enhanced manyfold both in F1 mouse splenocytes and serum compared with the parents (Figures 5F and 5G). Additionally, GEO dataset: NCBI's Genbank_GSE79240 (Wang et al., 2016) was utilized to observe the differential expression of microRNAs during SLE, especially miR-30e expression level, which further revealed that expression of miR-30e modestly enhanced in dendritic cells of patients with SLE (n = 5) compared with healthy controls (n = 5) (Figure S12A). To understand the relevance of miR-30e in another autoimmune disease, we reanalyzed the previously submitted GEO dataset (NCBI's Genbank_GSE55099) for patients with type 1 diabetes mellitus. The reanalysis unveils that the expression of miR-30e significantly enhanced in PBMCs of patients (n = 12) compared with healthy controls (n = 10) (Figure S12B). Collectively, these results suggest that enhanced innate immune responses are strongly linked with miR-30e expression under physiological condition and it might also play a pivotal role in immuno-pathogenesis of SLE in both human and mouse model.

The enhanced expression of inflammatory cytokines, type I IFNs, and type I IFN-inducible genes along with elevated miR-30e in patients with SLE and SLE mouse model prompted us to examine the levels of our previously identified negative regulators as shown (Figures 3A and 3B). Additionally, it has been reported that several negative regulators of innate immunity play a crucial role in the development of autoimmune diseases. As expected, the expression of negative regulators of PRR-mediated signaling pathways, namely, *TRIM38*, *TANK*, *SOCS1*, and *SOCS3* was significantly reduced in the PBMCs of patients with SLE compared with healthy controls (Figure 5H). To support our observation, reanalysis of previously submitted GEO dataset, NCBI's Genbank_GSE11909 (Chaussabel et al., 2008) for patients with SLE (n = 103) and healthy controls (n = 12) in PBMCs reveal that, in SLE, the identified negative regulators of innate immune signaling pathway that may be targeted by miR-30e were significantly reduced in patients (n = 103) compared with healthy controls (n = 12) (Figure S13A). To confirm our observations, splenocytes from mouse model were analyzed for identified negative regulators. Consistent with human result for the expression of negative regulators, the expression of *Atg5* and *Atg12* was significantly reduced, whereas expression of *Socs1* and *Socs3* was moderately reduced in SLE mouse (F1-NZW/B mice: n = 7) compared with parent mice (PM-NZW-NZB: n = 7) (Figure 5I). Collectively, these results suggest that, in SLE pathogenesis, in both human and mouse, enhanced expression of miR-30e might play a crucial role by suppressing the expression of negative regulators of innate immune signaling pathway, which in turn enhances innate immune cytokines and contributes to the development or severity of the disease. Therefore, manipulation of miR-30e expression might prove to be a key factor for controlling SLE pathogenesis.

Prognostic and Therapeutic Potential of miR-30e

To explore the prognostic and therapeutic potential of miR-30e, which modulates innate immune responses during infection and autoimmune diseases, particularly HBV infection and SLE, we tested the prognostic potential of miR-30e. We validated the miR-30e expression by comparing the serum levels in pre- and post 6 months therapy (pegylated type I interferon) samples of patients with HBV (demographic details mentioned in Table S5). Strikingly, we found significant reduction of miR-30e expression after interferon therapy (Figure 6A), suggesting that HBV infection triggers miR-30e over-expression in the host, which combats the virus infection, that is, otherwise ablates upon Peg-IFN treatment, a well-established therapy that reduces the hepatitis B virus titer in patients. Additionally, GEO dataset NCBI's Genbank_GSE104126 (Yang et al., 2018) supports the above finding in the context of miR-30e expression level, as its reanalysis revealed, that there was significant reduction in the level of miR-30e in pegylated type I

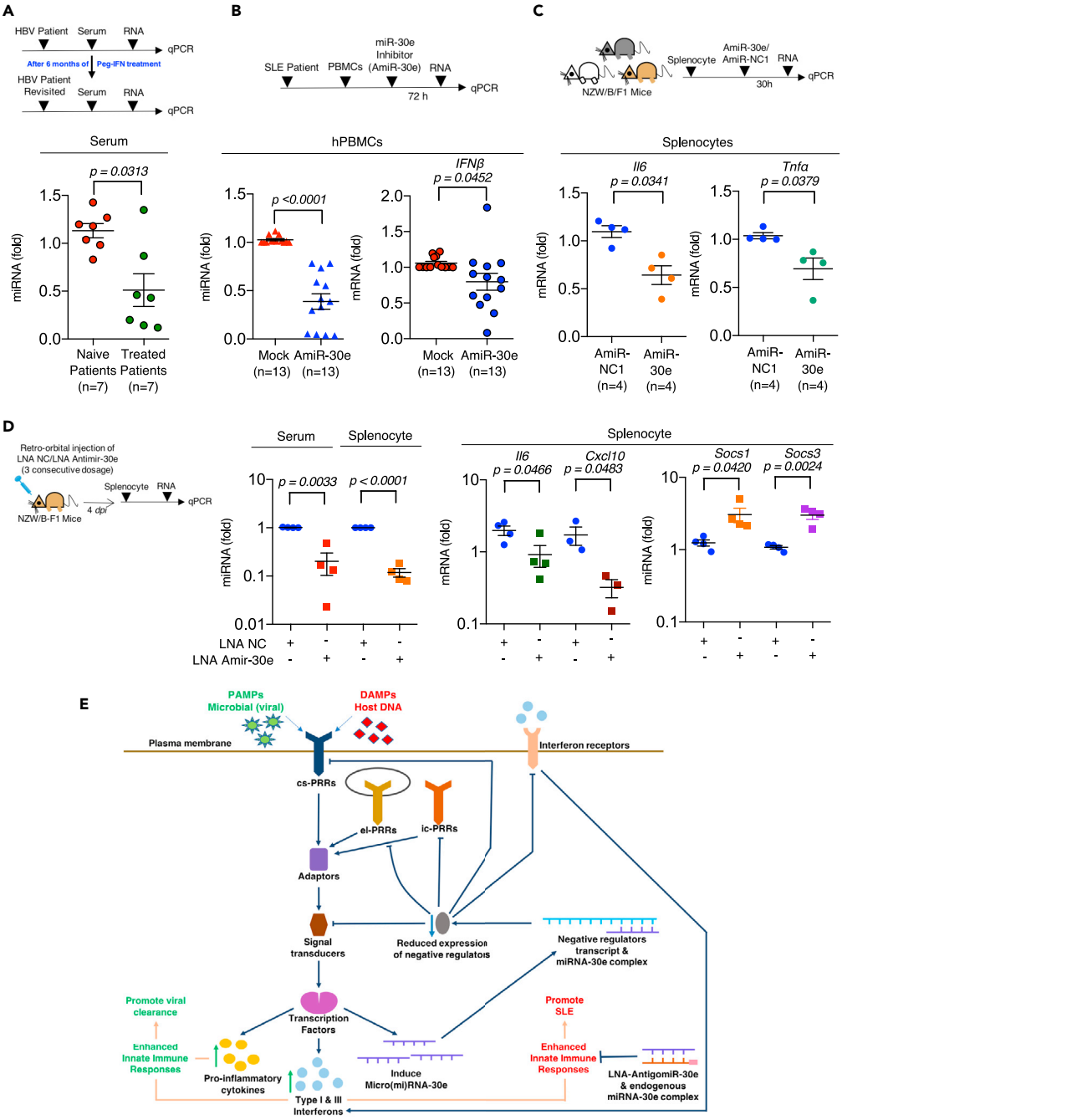

Figure 6. Prognostic and Therapeutic Potential of miR-30e

Figure360▷ For a Figure360 author presentation of this figure, see https://doi.org/10.1016/j.isci.2020.101322.

(A) Schematic representation of the workflow for quantification of the fold changes by qRT-PCR analysis of miR-30e as indicated, in the serum collected from hepatitis B (HBV) naive patients (n = 7) compared with HBV treated (with pegylated IFNs) patients (n = 7).

(B) Schematic representation of workflow for quantification of the fold changes in the relative abundances of miR-30e and *IFNβ* as indicated, in the PBMCs from patients with SLE treated with/without AmiR-30e (miR-30e inhibitor).

(C) Schematic representation of the *ex vivo* experiment workflow for quantification of the fold changes in the relative abundances of *Il6* and *Tnfα* as indicated, in the splenocytes from SLE mice model (as described previously) treated with AmiR-30e (miR-30e inhibitor) and AmiR-NC1.

(D) Schematic representation of the *in vivo* experiment workflow for quantification of the fold changes of miR-30e, *Il6*, *Cxcl10*, *Socs1*, and *Socs3* as indicated, in the splenocytes and serum from SLE mice model (as described previously); four

Figure 6. *Continued*

mice distributed in each group were subjected to LNA-miR-30e-antagomir (LNA Amir-30e) and LNA-negative control antagomir (LNA NC) treatment (explained in materials and methods). Data are mean ± SEM of triplicate samples from single experiment (A, B, and D) and are representative of two independent experiments (C). All the p values/***p < 0.001 defined by paired t test.

(E) Viral PAMPs (green) and DAMPs (red) sensed by pattern recognition receptors (PRRs) to activate cascade of innate immune signaling pathways, which induce pro-inflammatory cytokines (yellow), type I and type III interferons (sky blue), and miRNA-30e (purple). miRNA-30e regulates both PAMPs and DAMPs induced immune responses by targeting the 3′ UTR of negative regulators (dark blue) of innate immune signaling pathways and reducing the expression of these negative regulators (gray). During viral infection, miR-30e is induced, which reduces the cellular abundance of negative regulators to enhance innate immune responses and facilitate viral clearance. The endogenous host DNA induces miR-30e and subsequently enhances innate immune responses for the development of autoimmune disease, SLE. SLE signatory inhibition is shown by LNA-AntigomiR-30e and endogenous miR-30e complex.

See also Figure S14 and Table S5.

interferons treated and HBsAg-loss (reduction in viral titer) patients compared with pegylated type I interferons treated and non-HBsAg loss (no change in viral titer) patients (Figure S14).

Next, we investigated the therapeutic potential of miR-30e modulator and have shown the importance of AmiR-30e (miR-30e inhibitor) that sequesters the activity of endogenous miR-30e. Our results showed that patients with SLE and mouse model produce high inflammatory responses in terms of innate cytokines and it is linked to the elevated miR-30e expression (Figures 5A–5G) and contributes to the reduction of negative regulators (Figures 5H and 5I). Therefore, we introduce AmiR-30e into PBMCs of patients with SLE. Interestingly, we found that ectopic expression of AmiR-30e sequesters the expression of miR-30e in PBMCs of patients with SLE and reduces the *IFNβ* expression as quantified by qRT-PCR (Figure 6B). Next, we examined the role of AmiR-30e in SLE mouse model, NZW/B. In an *ex vivo* experiment, transfection of splenocytes, derived from the F1 mice (NZW/B), with AmiR-30e significantly reduces the expression levels of *Il6* and *Tnfα* compared with the control AmiR-NC1 (Figure 6C). Furthermore, to show the stable and specific sequestering effects of microRNAs for therapeutic relevance, we found that previously it was reported that locked nucleic acid (LNA)-based chemistry to design a potent inhibitor against the microRNA has showed promising effects in *in vivo* studies (Garchow et al., 2011). Therefore we finally performed *in vivo* experiments to test the effects of LNA-anti-mir-30e-5p (LNA Amir-30e) on innate immune responses in SLE mice. The two groups of mice, each consisting of four mice, were injected with LNA Amir-30e or LNA negative control (LNA NC) through retro-orbital route thrice with 1-day interval to sequester the endogenous expression of mir-30e, to measure the abundance of mir-30e and related genes. The expression of mir-30e in serum and splenocytes of SLE induced F1 (NZW/B) mice was significantly reduced compared with the LNA NC treated mice. Additionally, innate immune cytokines, namely, *Il6* and *Cxcl10*, significantly reduced in LNA Amir-30e-treated mice compared with the LNA NC. In contrast, the expression of negative regulators, *Socs1* and *Socs3*, significantly enhanced in LNA Amir-30e-treated mice compared with the LNA NC (Figure 6D). Taken together these findings conclude that LNA Amir-30e was stable under *in vivo* conditions and significantly inhibits the activity of mir-30e in SLE mouse model, which further reduces the inhibition/targeting of negative regulators, contributing toward controlling of SLE phenomena. Overall, our study presents the involvement of miR-30e and its inhibition in two of the challenging diseases, virus infections and autoimmune disorder, through a common axis of mechanism, summarized in Figure 6E.

DISCUSSION

Innate immune responses to viral infection induce the production of pro-inflammatory cytokines and type I interferons (IFNs) through a cascade of complex signaling pathways that play critical roles in development of appropriate anti-viral immunity. In contrast, dysregulation of these signaling pathways results in inefficient clearance of microbial infection, immunopathology, or autoimmune diseases (Akira et al., 2006; He and Hannon, 2004). Therefore, the expression and activation of signaling molecules in signaling pathways are tightly regulated at transcriptional, post-transcriptional, translational, and post-translational levels. The non-coding small (micro) RNAs play a pivotal role in fine-tuning of protein coding genes through affecting the stability and modulating the translation of gene transcripts. Here, our study identifies a novel role of miR-30e in the regulation of innate immune signaling pathway during virus infections (chronic infection, such as HBV) and immuno-pathogenesis of autoimmune disorder, SLE. We also demonstrated the

therapeutic and prognostic potential of miR-30e inhibition by AmiR-30e (antagomir-30e) and miR-30e in SLE and HBV infection, respectively.

The miR-30e was identified through unbiased *in silico* screening using GEO datasets obtained from cell lines, primary cells, mice, or human patients challenged by different viruses. Although other miRNAs such as miR-27a-3p and miR-181a/2-3p were also induced, however, their complementation potency toward mRNA-miRNA targets was manyfold lower than that of miR-30e. The miR-30e has been reported to be associated with cancer (Ning et al., 2017; Feng et al., 2017; Liu et al., 2017), cardiac dysfunction (Su et al., 2018), kidney malfunction (Wu et al., 2015), fatty acid deregulation, as a biomarker for SLE (Kim et al., 2016), a dysregulated micro RNA during Zika virus infection (Kozak et al., 2017), and suppressor for Dengue virus (Zhu et al., 2014). However, its role in innate immune signaling pathway and innate immune responses during virus infections and pathogenesis of autoimmune diseases such as SLE remains unclear.

Our results showed that miR-30e induced manyfold in the serum of (n = 51) therapy-naive patients with chronic hepatitis B (CHB) compared with healthy control (n = 24). This finding was also supported by other DNA and RNA virus, such as HCMV, NDV, and SeV, infection or stimulation with TLRs or RLRs viral PAMPs, such as ssRNA and poly I:C of various cell lines. Ectopic expression of miR-30e in primary cells or cell lines upon subsequent DNA or RNA virus infection significantly reduces the viral load through global enhancement of innate immune responses in terms of pro-inflammatory cytokines, type I interferons, and type I interferon-inducible genes as shown by NGS data analysis. The enhanced miR-30e expression in therapy-naive HBV (CHB) patients might elevate innate immune responses to combat HBV infection; however, it might be insufficient to control HBV infection. Therefore, patients with HBV receiving pegylated interferon were sampled after 6 months of therapy and were found to show significant reduction of viral load and miR-30e expression highlighting the link between HBV, miR-30e, and innate immune responses. To establish the role of miR-30e under physiological condition, we selected SLE as a disease model. Patients with SLE show enhanced expression of miR-30e, pro-inflammatory cytokines, type-I interferons, or type-I interferon-inducible genes. Further to confirm our observations, we exploited SLE mouse model (NZW/NZB F1) (Morel, 2010) and obtained similar results for the expression of miR-30e that were consistent with the results of patients with SLE, suggesting the correlation of miR-30e with innate immune responses in SLE under physiological condition.

The transcriptomic analysis of our NGS data and GEO datasets using various bioinformatics tools shows that miR-30e directly targets several signal transducers and the negative regulators such as *TRIM38* (Versteeg et al., 2014; Zhao et al., 2012; Hu et al., 2014), *TANK* (Kawagoe et al., 2009), *ATG5*, *ATG12* (Li et al., 2018; Jounai et al., 2007), *BECN1* (Cui et al., 2016), *SOCS1*, and *SOCS3* (Pothlichet et al., 2008) validated in the study and few others *TRIM35* (Wang et al., 2015), *TRIM13* (Narayan et al., 2014), and *EPG5* (Lu et al., 2016) discussed in Table S2. The microRNA targeting reduces the expression of negative regulators and enhances the innate immune responses that play a pivotal role in TLR, RLR, NLR, and type I interferon signaling pathways. Although miR-30e also binds with few other gene transcripts that are not the negative regulators in the innate immune signaling pathways, the combined mean free energy for these transcripts are lower than the threshold binding energy necessary for significant change in the expression of transcripts, for subsequently affecting the outcome of signaling pathways. Notably, the expression of negative regulators such as *TRIM38*, *TANK*, *SOCS1*, and *SOCS3* in patients with SLE are significantly reduced. Moreover, SLE mice also showed similar results for the expression of *Socs1*, *Socs3*, *Atg5*, and *Atg12*. Collectively, human and mouse results illustrate that miR-30e targets negative regulators to elevate innate immune responses and dysregulation of miR-30e expression might be one of the factors for the establishment of SLE or probably other autoimmune diseases.

Previously, it has been shown that patients with SLE have reduced ability to degrade DNA and cellular chromatin (Gheita et al., 2018). DAMPs, specially the double-stranded (ds)DNA, are considered to be associated with the lupus as mentioned in the introductory section of the study and could be utilized to study the SLE-related cellular phenomena by adopting simple experimental techniques. The dsDNA could mimic the self-DNA of lupus-associated outcomes and results in modulating the inflammatory/immune responses, cell death, which were conventionally considered as the signatory and/or onset features associated with SLE pathogenesis. Therefore, PBMCs from healthy donors were stimulated with partially degraded self-DNA, and these cells showed enhanced miR-30e expression and innate immune responses suggesting the pathogenic role of miR-30e, which suggests the association of self-DNA with the

pathogenesis of SLE. In contrast, sequestering the endogenous miR-30e in PBMCs of patients with SLE by introducing antagomir/inhibitor or miR-30e significantly reduced the levels of miR-30e and innate immune responses in terms of *IFNβ* production. Additionally, the introduction of locked nucleic acid-based inhibitor of miR-30e (a stable form of antagomir) through retro-orbital route into SLE mice model significantly reduced mir-30e and innate immune genes expression in splenocytes, whereas expression of some of the negative regulators was moderately enhanced, demonstrating the ability of mir-30e antagomir/inhibitor to reduce the innate immune responses under physiological condition. Overall, our study identified miR-30e as a post-transcriptional regulator of negative regulation of PRR-mediated innate immune signaling pathways and its prognostic potential in virus infections, such as HBV infection. Additionally, our study demonstrated the therapeutic implications of miR-30e antagomir/inhibitor in immunologically complex autoimmune disease, SLE, or possibly other autoimmune diseases.

Limitations of the Study

The limitation of the study is the exclusion of *in vivo* experiments for the mechanism of induction of miR-30e-5p, using various knockout mice such as *TLR/MyD88/TRIF/IPS-1* or *STING*. Knockout mice inclusion will provide the mechanistic insight for miR-30e-5p induction in viral infections and/or SLE. Another limitation is the exclusion of data demonstrating the reduction of the negative regulator at protein levels in several primary cells because of the limitation of survival of primary cell due to the introduction of miR-30e-5p and subsequent virus infections. Though in this work, we have demonstrated the reduction of negative regulators *in vivo* at the transcript levels. Additionally, serum samples collected from the patients could also be normalized, for the quantification of microRNAs, by using more than one internal control along with conventional RNU6 (U6) internal control to avoid any challenge in disseminating the patient-related data.

Resources Availability

Lead Contact

Further information and requests for resources and reagents should be directed to and will be fulfilled by the Lead Contact, Himanshu Kumar (hkumar@iiserb.ac.in).

Material Availability

The study did not generate any unique reagent/s.

Data and Code Availability

The NGS (RNA sequencing [RNA-seq]) data for expression profiling reported in this paper have been deposited in the GenBank database (accession no. NCBI's Genbank_GSE130005).

METHODS

All methods can be found in the accompanying Transparent Methods supplemental file.

SUPPLEMENTAL INFORMATION

Supplemental Information can be found online at https://doi.org/10.1016/j.isci.2020.101322.

ACKNOWLEDGMENTS

We thank Dr. Takaji Wakita for providing the HepG2-NTCP cell lines. We thank Dr. Nirupma Trehanpati and Dr. Senthil Kumar Venugopal for providing the HepG2 and HepG2215 cell lines. We thank Dr. Sunil Raghav for providing Sendai-RFP, Professor Peter Palese for providing NDV-GFP, and Professor Wade Gibson for providing HCMV-GFP and HFFs. We thank Professor T. Tuschl for providing the Ago2-Flag construct through Addgene and BEI Resources for providing human *rh-IFNβ*. We thank Dr. Harshad Ingle for proofreading and helping with illustrating the graphical abstract. We are extremely thankful to Dr. Nachimuthu Senthil Kumar for his financial support of the work, under the grant (BT/PR25052/NER/95/983/2017) jointly given to N.S.K. and H.K. We are grateful to Indian Institute of Science Education and Research (IISER) Bhopal for providing the Central Instrumentation Facility. We also thank all members of the laboratory for helpful discussions. Finally, we are eternally grateful to all the patients and healthy donors for proving their blood samples for the study.

Funding: This work was partially supported by IISER Bhopal–IGM Hokkaido University Grant for General Joint Research Program of the Institute for Genetic Medicine, Hokkaido University, Japan, and by an Intramural Research Grant of IISER, Bhopal, India, to H.K. Start-up grant, IISER Bhopal to A.C. Extramural grant from ICMR (5/8/4-3/Env11/NCD-I) to P.G. R.M. is supported by the IISER Bhopal institutional fellowship.

AUTHOR CONTRIBUTIONS

Conceptualization, R.M. and H.K.; Investigation, R.M., S.S., and B.S.R.; Validation, R.M., S.S., S.B., D.K., and As.K.; Formal Analysis, R.M., K.N., and H.K.; Data Curation, Ak.K. and R.M.; Writing – Original Draft, R.M. and H.K.; Writing – Review & Editing, R.M. and H.K.; Project Administration, P.G., A.A., P.T., A.T., and H.K.; Funding Acquisition, A.C., P.G., A.T., and H.K.; Resources, P.G., A.A., P.T., and A.T.; Supervision, H.K.

DECLARATION OF INTERESTS

The authors declare no competing interests.

Received: February 4, 2020
Revised: May 26, 2020
Accepted: June 25, 2020
Published: July 24, 2020

REFERENCES

Akira, S., Uematsu, S., and Takeuchi, O. (2006). Pathogen recognition and innate immunity. Cell *124*, 783–801.

Alvarez, K., and Vasquez, G. (2017). Damage-associated molecular patterns and their role as initiators of inflammatory and auto-immune signals in systemic lupus erythematosus. Int. Rev. Immunol. *36*, 259–270.

Chaussabel, D., Quinn, C., Shen, J., Patel, P., Glaser, C., Baldwin, N., Stichweh, D., Blankenship, D., LI, L., Munagala, I., et al. (2008). A modular analysis framework for blood genomics studies: application to systemic lupus erythematosus. Immunity *29*, 150–164.

Cui, J., Jin, S., and Wang, R.F. (2016). The BECN1-USP19 axis plays a role in the crosstalk between autophagy and antiviral immune responses. Autophagy *12*, 1210–1211.

Devarapu, S.K., and Anders, H.J. (2018). Toll-like receptors in lupus nephritis. J. Biomed. Sci. *25*, 35.

Feng, G.X., Li, J., Yang, Z., Zhang, S.Q., Liu, Y.X., Zhang, W.Y., Ye, L.H., and Zhang, X.D. (2017). Hepatitis B virus X protein promotes the development of liver fibrosis and hepatoma through downregulation of miR-30e targeting P4HA2 mRNA. Oncogene *36*, 6895–6905.

Gao, L., Ai, J., Xie, Z., Zhou, C., Liu, C., Zhang, H., and Shen, K. (2015). Dynamic expression of viral and cellular microRNAs in infectious mononucleosis caused by primary Epstein-Barr virus infection in children. Virol. J. *12*, 208.

Garchow, B.G., Bartulos Encinas, O., Leung, Y.T., Tsao, P.Y., Eisenberg, R.A., Caricchio, R., Obad, S., Petri, A., Kauppinen, S., and Kiriakidou, M. (2011). Silencing of microRNA-21 in vivo ameliorates autoimmune splenomegaly in lupus mice. EMBO Mol. Med. *3*, 605–615.

Gheita, T.A., Abaza, N.M., Hammam, N., Mohamed, A.A.A., El, G.; II, and Eissa, A.H. (2018). Anti-dsDNA titre in female systemic lupus erythematosus patients: relation to disease manifestations, damage and antiphospholipid antibodies. Lupus *27*, 1081–1087.

He, L., and Hannon, G.J. (2004). MicroRNAs: small RNAs with a big role in gene regulation. Nat. Rev. Genet. *5*, 522–531.

Hu, M.M., Yang, Q., Zhang, J., Liu, S.M., Zhang, Y., Lin, H., Huang, Z.F., Wang, Y.Y., Zhang, X.D., Zhong, B., and Shu, H.B. (2014). TRIM38 inhibits TNFalpha- and IL-1beta-triggered NF-kappaB activation by mediating lysosome-dependent degradation of TAB2/3. Proc. Natl. Acad. Sci. U S A *111*, 1509–1514.

Ingle, H., Kumar, S., Raut, A.A., Mishra, A., Kulkarni, D.D., Kameyama, T., Takaoka, A., Akira, S., and Kumar, H. (2015). The microRNA miR-485 targets host and influenza virus transcripts to regulate antiviral immunity and restrict viral replication. Sci. Signal. *8*, ra126.

Jounai, N., Takeshita, F., Kobiyama, K., Sawano, A., Miyawaki, A., Xin, K.Q., Ishii, K.J., Kawai, T., Akira, S., Suzuki, K., and Okuda, K. (2007). The Atg5 Atg12 conjugate associates with innate antiviral immune responses. Proc. Natl. Acad. Sci. U S A *104*, 14050–14055.

Kawagoe, T., Takeuchi, O., Takabatake, Y., Kato, H., Isaka, Y., Tsujimura, T., and Akira, S. (2009). TANK is a negative regulator of Toll-like receptor signaling and is critical for the prevention of autoimmune nephritis. Nat. Immunol. *10*, 965–972.

Kim, B.S., Jung, J.Y., Jeon, J.Y., Kim, H.A., and Suh, C.H. (2016). Circulating hsa-miR-30e-5p, hsa-miR-92a-3p, and hsa-miR-223-3p may be novel biomarkers in systemic lupus erythematosus. HLA *88*, 187–193.

Kim, S., Seo, D., Kim, D., Hong, Y., Chang, H., Baek, D., Kim, V.N., Lee, S., and Ahn, K. (2015). Temporal landscape of MicroRNA-mediated host-virus crosstalk during productive human cytomegalovirus infection. Cell Host Microbe *17*, 838–851.

Kondo, T., Kawai, T., and Akira, S. (2012). Dissecting negative regulation of Toll-like receptor signaling. Trends Immunol. *33*, 449–458.

Kozak, R.A., Majer, A., Biondi, M.J., Medina, S.J., Goneau, L.W., Sajesh, B.V., Slota, J.A., Zubach, V., Severini, A., Safronetz, D., et al. (2017). MicroRNA and mRNA dysregulation in astrocytes infected with Zika virus. Viruses *9*, 297.

Li, M., Li, J., Zeng, R., Yang, J., Liu, J., Zhang, Z., Song, X., Yao, Z., Ma, C., Li, W., et al. (2018). Respiratory syncytial virus replication is promoted by autophagy-mediated inhibition of apoptosis. J. Virol. *92*, e02193–17.

Liu, M.M., Li, Z., Han, X.D., Shi, J.H., Tu, D.Y., Song, W., Zhang, J., Qiu, X.L., Ren, Y., and Zhen, L.L. (2017). MiR-30e inhibits tumor growth and chemoresistance via targeting IRS1 in Breast Cancer. Sci. Rep. *7*, 15929.

Lovgren, T., Eloranta, M.L., Bave, U., Alm, G.V., and Ronnblom, L. (2004). Induction of interferon-alpha production in plasmacytoid dendritic cells by immune complexes containing nucleic acid released by necrotic or late apoptotic cells and lupus IgG. Arthritis Rheum. *50*, 1861–1872.

Lu, Q., Yokoyama, C.C., Williams, J.W., Baldridge, M.T., Jin, X., Desrochers, B., Bricker, T., Wilen, C.B., Bagaitkar, J., Loginicheva, E., et al. (2016). Homeostatic control of innate lung inflammation by vici syndrome gene Epg5 and additional autophagy genes promotes influenza pathogenesis. Cell Host Microbe *19*, 102–113.

Magna, M., and Pisetsky, D.S. (2015). The role of cell death in the pathogenesis of SLE: is pyroptosis the missing link? Scand. J. Immunol. *82*, 218–224.

Mevorach, D. (2003). Systemic lupus erythematosus and apoptosis: a question of balance. Clin. Rev. Allergy Immunol. *25*, 49–60.

Morel, L. (2010). Genetics of SLE: evidence from mouse models. Nat. Rev. Rheumatol. *6*, 348–357.

Moulton, V.R., Suarez-Fueyo, A., Meidan, E., Li, H., Mizui, M., and Tsokos, G.C. (2017). Pathogenesis of human systemic lupus erythematosus: a cellular perspective. Trends Mol. Med. *23*, 615–635.

Munoz, L.E., van Bavel, C., Franz, S., Berden, J., Herrmann, M., and van der Vlag, J. (2008). Apoptosis in the pathogenesis of systemic lupus erythematosus. Lupus *17*, 371–375.

Narayan, K., Waggoner, L., Pham, S.T., Hendricks, G.L., Waggoner, S.N., Conlon, J., Wang, J.P., Fitzgerald, K.A., and Kang, J. (2014). TRIM13 is a negative regulator of MDA5-mediated type I interferon production. J. Virol. *88*, 10748–10757.

Ning, Z.Q., Lu, H.L., Chen, C., Wang, L., Cai, W., Li, Y., Cao, T.H., Zhu, J., Shu, Y.Q., and Shen, H. (2017). MicroRNA-30e reduces cell growth and enhances drug sensitivity to gefitinib in lung carcinoma. Oncotarget *8*, 4572–4581.

Porritt, R.A., and Hertzog, P.J. (2015). Dynamic control of type I IFN signalling by an integrated network of negative regulators. Trends Immunol. *36*, 150–160.

Pothlichet, J., Chignard, M., and Si-Tahar, M. (2008). Cutting edge: innate immune response triggered by influenza A virus is negatively regulated by SOCS1 and SOCS3 through a RIG-I/IFNAR1-dependent pathway. J. Immunol. *180*, 2034–2038.

Ronnblom, L., and Leonard, D. (2019). Interferon pathway in SLE: one key to unlocking the mystery of the disease. Lupus Sci. Med. *6*, e000270.

Shen, N., Liang, D., Tang, Y., de Vries, N., and Tak, P.P. (2012). MicroRNAs–novel regulators of systemic lupus erythematosus pathogenesis. Nat. Rev. Rheumatol. *8*, 701–709.

Su, Q., Ye, Z., Sun, Y., Yang, H., and Li, L. (2018). Relationship between circulating miRNA-30e and no-reflow phenomenon in STEMI patients undergoing primary coronary intervention. Scand. J. Clin. Lab Invest. *78*, 318–324.

Treiber, T., Treiber, N., and Meister, G. (2019). Regulation of microRNA biogenesis and its crosstalk with other cellular pathways. Nat. Rev. Mol. Cell Biol. *20*, 5–20.

Vela, E.M., Kasoji, M.D., Wendling, M.Q., Price, J.A., Knostman, K.A.B., Bresler, H.S., and Long, J.P. (2014). MicroRNA expression in mice infected with seasonal H1N1, swine H1N1 or highly pathogenic H5N1. J. Med. Microbiol. *63*, 1131–1142.

Versteeg, G.A., Benke, S., Garcia-Sastre, A., and Rajsbaum, R. (2014). InTRIMsic immunity: positive and negative regulation of immune signaling by tripartite motif proteins. Cytokine Growth Factor Rev. *25*, 563–576.

Wang, Y., Liang, J., Qin, H., Ge, Y., Du, J., Lin, J., Zhu, X., Wang, J., and Xu, J. (2016). Elevated expression of miR-142-3p is related to the pro-inflammatory function of monocyte-derived dendritic cells in SLE. Arthritis Res. Ther. *18*, 263.

Wang, Y., Yan, S., Yang, B., Wang, Y., Zhou, H., Lian, Q., and Sun, B. (2015). TRIM35 negatively regulates TLR7- and TLR9-mediated type I interferon production by targeting IRF7. FEBS Lett. *589*, 1322–1330.

Wu, J., Zheng, C., Wang, X., Yun, S., Zhao, Y., Liu, L., Lu, Y., Ye, Y., Zhu, X., Zhang, C., et al. (2015). MicroRNA-30 family members regulate calcium/calcineurin signaling in podocytes. J. Clin. Invest. *125*, 4091–4106.

Yang, Y., Liu, M., Deng, Y., Guo, Y., Zhang, X., Xiang, D., Jiang, L., You, Z., Wu, Y., Li, M., and Mao, Q. (2018). Pretreatment microRNA levels can predict HBsAg clearance in CHB patients treated with pegylated interferon alpha-2a. Virol. J. *15*, 73.

Yu, S.L., Kuan, W.P., Wong, C.K., Li, E.K., and Tam, L.S. (2012). Immunopathological roles of cytokines, chemokines, signaling molecules, and pattern-recognition receptors in systemic lupus erythematosus. Clin. Dev. Immunol. *2012*, 715190.

Zhao, W., Wang, L., Zhang, M., Yuan, C., and Gao, C. (2012). E3 ubiquitin ligase tripartite motif 38 negatively regulates TLR-mediated immune responses by proteasomal degradation of TNF receptor-associated factor 6 in macrophages. J. Immunol. *188*, 2567–2574.

Zheng, Z., Ke, X., Wang, M., He, S., Li, Q., Zheng, C., Zhang, Z., Liu, Y., and Wang, H. (2013). Human microRNA hsa-miR-296-5p suppresses enterovirus 71 replication by targeting the viral genome. J. Virol. *87*, 5645–5656.

Zhu, X., He, Z., Hu, Y., Wen, W., Lin, C., Yu, J., Pan, J., Li, R., Deng, H., Liao, S., et al. (2014). MicroRNA-30e* suppresses dengue virus replication by promoting NF-kappaB-dependent IFN production. PLoS Negl. Trop. Dis. *8*, e3088.

iScience, Volume *23*

Supplemental Information

MicroRNA-30e-5p has an Integrated Role in the Regulation of the Innate Immune Response during Virus Infection and Systemic Lupus Erythematosus

Richa Mishra, Sanjana Bhattacharya, Bhupendra Singh Rawat, Ashish Kumar, Akhilesh Kumar, Kavita Niraj, Ajit Chande, Puneet Gandhi, Dheeraj Khetan, Amita Aggarwal, Seiichi Sato, Prafullakumar Tailor, Akinori Takaoka, and Himanshu Kumar

Supplementary Information

1. Supplementary Figures and Tables

2. Transparent Methods

Figure. S1

A

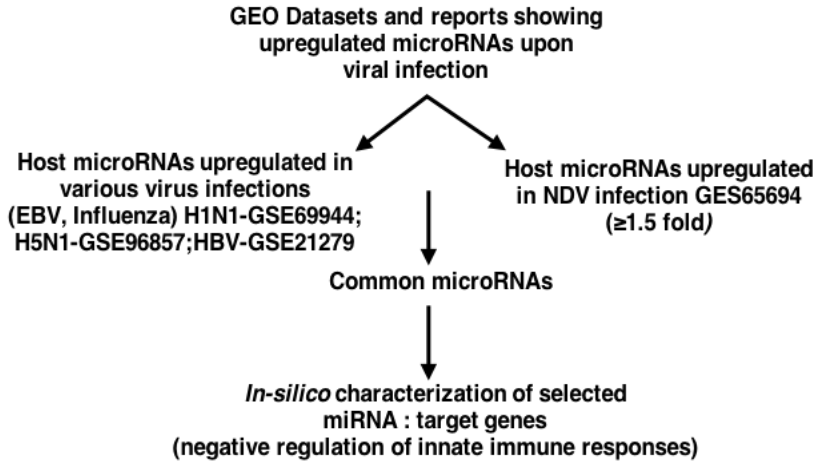

B

S.No.	Viral Infection	Model or Cell line	Upregulated miRs	Reference
1.	H5N1	Mice	51	(Vela et al., 2014)
2.	EBV	Patients (IM)	84	(Gao et al., 2015)
3.	NDV	HEK-293	209	(Ingle et al., 2015)

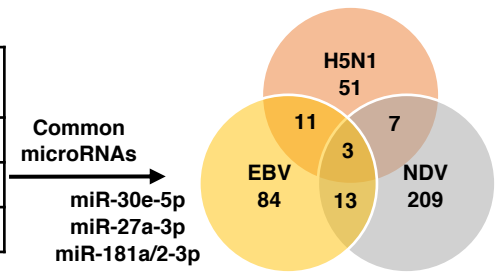

C

miRNA	Log FC during NDV Infection GSE65694	Negative Regulation of Innate Immune Responses (miRanda, DIANA, TargetScan, miRDB, RNA hybrid)
miR-30e-5p	1.69	**** (majority of targets with high binding efficiency towards miRNAs)
miR-27a-3p	1.54	*
miR-181a/2-3p	1.5	*

(*) - Significant targeting by miRNA

Common microRNA

miR-30e-5p

D

```
                5′ ********    3′
hsa-miR-30e-5p  UGUAAACAUCCUU
mmu-miR-30e-5p  UGUAAACAUCCUU
rno-miR-30e-5p  UGUAAACAUCCUU
mml-miR-30e-5p  UGUAAACAUCCUU
gga-miR-30e-5p  UGUAAACAUCCUU
chi-miR-30e-5p  UGUAAACAUCCUU
dre-miR-30e-5p  UGUAAACAUCCUU
bta-miR-30e-5p  UGUAAACAUCCUU
```

E (i)

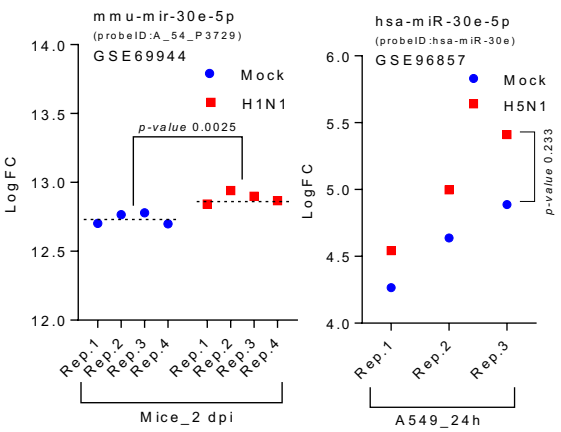

F

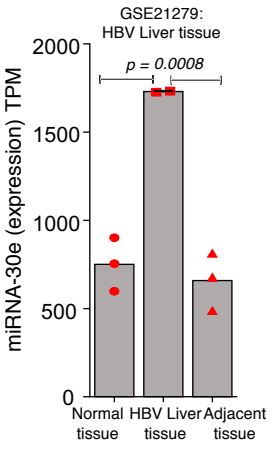

Figure S1 - miRNA-30e induced during viral infection, Related to Figure 1. (A) Schematic representation for the selection and screening pipeline of common miRNAs during viral infections. (B) Table and Venn diagram represent miR-30e-5p, miR-27a-3p and miR-181a/2-3p as commonly upregulated miRNAs during indicated infections. Abundance of miR-30e-5p as log fold change (Log FC) and transcripts per million (TPM) in indicated infections, (C) Log FC (fold change) of the selected miRNAs and efficiency (represented by [*] asterisk) by which they target the negative regulation of innate immune signaling pathways as per indicated GEO dataset (GSE65694) and algorithms. (D) miR-30e is conserved among the wide range of species (green); hsa, Homo sapiens (Human); mmu, *Mus musculus (Mouse)*; rno, *Rattus norvegicus (Norway Rat)*; mml, *Macaca mulatta (Rhesus monkey)*; gga, *Gallus gallus (chicken); chi, Capra hircus (Goat); dre, Danio rerio (Zebrafish) and bta, Bos Taurus (Cattle).*

Figure. S2

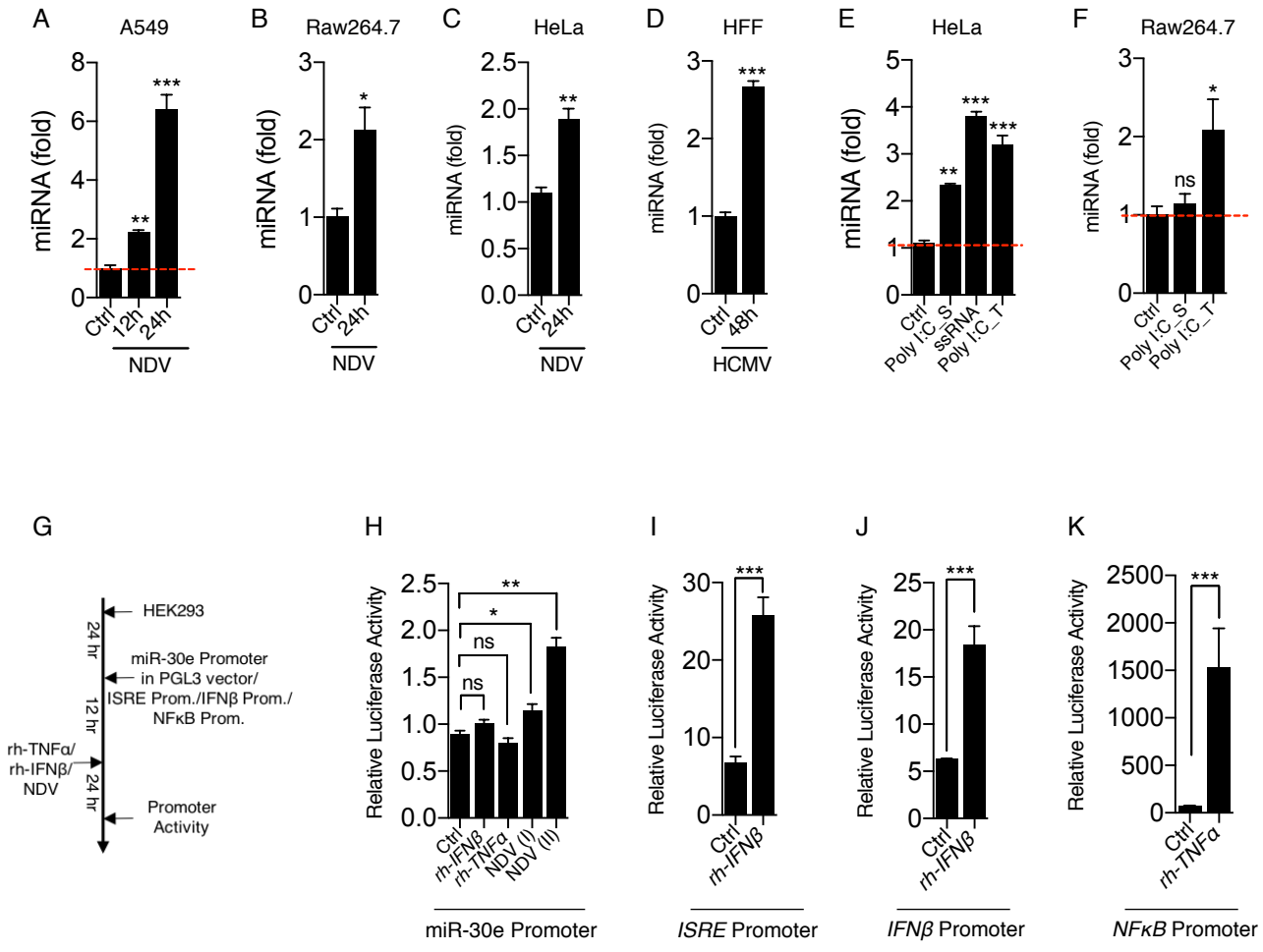
A
A549
miRNA (fold)
Ctrl
12h
24h
NDV
B
Raw264.7
Ctrl
24h
NDV
C
HeLa
Ctrl
24h
NDV
D
HFF
Ctrl
48h
HCMV
E
HeLa
Ctrl
Poly I:C_S
ssRNA
Poly I:C_T
F
Raw264.7
ns
Ctrl
Poly I:C_S
Poly I:C_T
G
HEK293
24 hr
miR-30e Promoter
in PGL3 vector/
ISRE Prom./IFNβ Prom./
NFκB Prom.
12 hr
rh-TNFα/
rh-IFNβ/
NDV
24 hr
Promoter
Activity
H
Relative Luciferase Activity
ns
Ctrl
rh-IFNβ
rh-TNFα
NDV (I)
NDV (II)
miR-30e Promoter
I
Relative Luciferase Activity
Ctrl
rh-IFNβ
ISRE Promoter
J
Relative Luciferase Activity
Ctrl
rh-IFNβ
IFNβ Promoter
K
Relative Luciferase Activity
Ctrl
rh-TNFα
NFκB Promoter

Figure S2 - Induction of miRNA-30e in different cells by DNA, RNA virus and viral PAMPs, Related to Figure 1. (A-F) Quantification of the fold changes by qRT-PCR in the abundances of miR-30e (at the indicated times and cells) after indicated viral infections and viral PAMPs treatment (A-C) NDV (MOI 5) in A549, Raw 264.7 and HeLa cells respectively, (D) HCMV-GFP (MOI 5) in HFF. (E and F) indicated synthetic PAMPs [poly IC (10μg/ml) {stimulation (S) and transfection (T)}; ssRNA (2μg/ml)] in (E) HeLa and (F) Raw 264.7 cells. (G) Schematic representation of workflow for quantification of miR-30e promoter activity and ISRE/IFNβ/NFκB promoter activity by luciferase assay as indicated in (H-K) HEK293 cells. NDV(I) is 5 MOI and NDV(II) is 10 MOI. rh = Recombinant. Data are mean +/- SEM of triplicate samples from single experiment and are representative of three (A-C, E-F and I-M) two (D and H) independent experiments. ***$P<0.001$, **$P<0.01$ and *$P<0.05$ by one-way ANOVA Tukey test and unpaired t-test.

Figure. S3

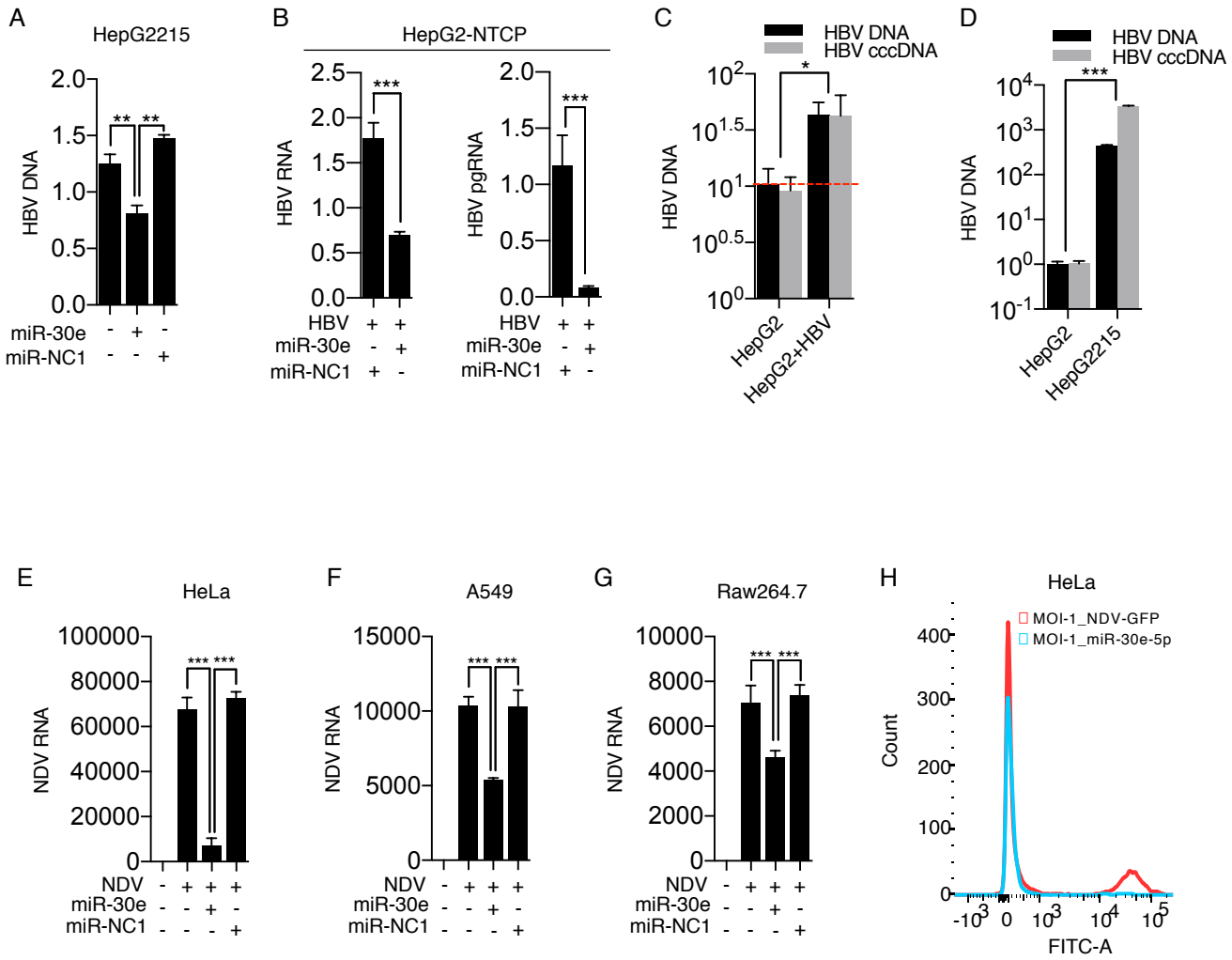
A
HepG2215
HBV DNA
2.0
1.5
1.0
0.5
0.0
**
**
miR-30e - + -
miR-NC1 - - +
B
HepG2-NTCP
HBV RNA
2.5
2.0
1.5
1.0
0.5
0.0
***
HBV + +
miR-30e - +
miR-NC1 + -
HBV pgRNA
2.0
1.5
1.0
0.5
0.0
***
HBV + +
miR-30e - +
miR-NC1 + -
C
HBV DNA
HBV cccDNA
HBV DNA
10^2
$10^{1.5}$
10^1
$10^{0.5}$
10^0
*
HepG2
HepG2+HBV
D
HBV DNA
HBV cccDNA
HBV DNA
10^4
10^3
10^2
10^1
10^0
10^{-1}
***
HepG2
HepG2215
E
HeLa
NDV RNA
100000
80000
60000
40000
20000
0
*** ***
NDV - + + +
miR-30e - - + -
miR-NC1 - - - +
F
A549
NDV RNA
15000
10000
5000
0
*** ***
NDV - + + +
miR-30e - - + -
miR-NC1 - - - +
G
Raw264.7
NDV RNA
10000
8000
6000
4000
2000
0
*** ***
NDV - + + +
miR-30e - - + -
miR-NC1 - - - +
H
HeLa
MOI-1_NDV-GFP
MOI-1_miR-30e-5p
Count
400
300
200
100
0
-10^3 0 10^3 10^4 10^5
FITC-A

Figure S3 - miR-30e inhibits viral replication, Related to Figure 1. (A-G) Quantification of the fold changes in the relative abundances of viral transcripts measured by qRT-PCR after the infection in indicated cells (A) HepG2215 cells were transfected with miR-30e and miR-NC1 as described previously, (B) HepG2-NTCP cells were transfected with miR-30e and miR-NC1 to quantify the relative expression (RE) of HBV viral transcripts (HBV RNA and pgRNA), (C-D) HBV patient's serum used to infect HepG2 compared with HepG2215 cells as indicated. (E-G) HeLa, A549 and Raw264.7 cells were transfected with miR-30e or miR-NC1 respectively prior to NDV infection as described previously. (H) Quantification of NDV viral signals detected by flow cytometry in HeLa cells, mock transfected or transfected with miR-30e for 24 hours then subjected to NDV (GFP tagged) infection (MOI 5) for 24 hours. HBV DNA and HBV cccDNA represent different primers set used to measure HBV viral transcripts. Data are mean +/- SEM of triplicate samples from single experiment and are representative of three (E-G) two (A-D and H) independent experiments. ***$P<0.001$ and **$P<0.01$ by one-way ANOVA Tukey test and unpaired t-test.

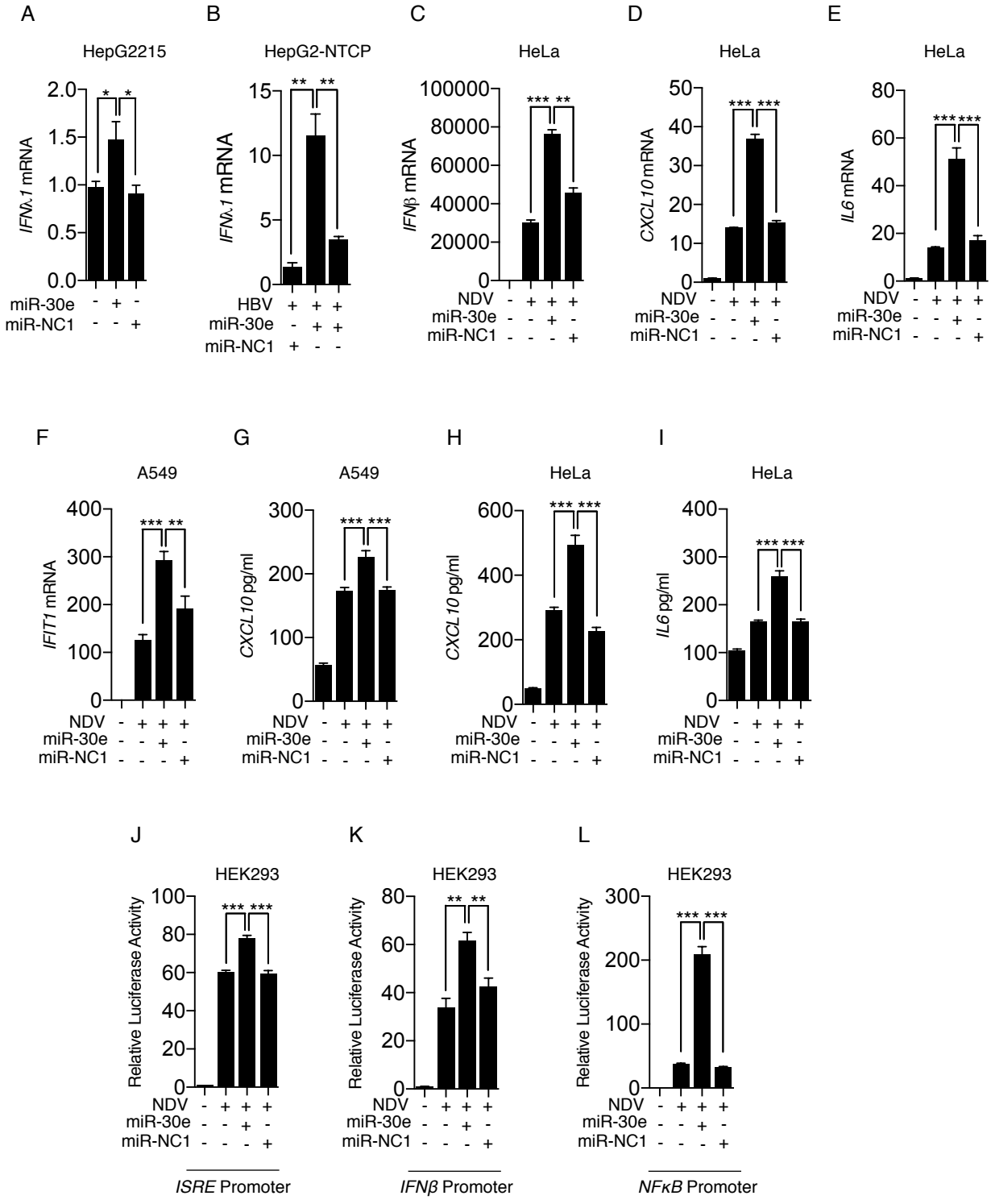
A
HepG2215
IFNλ1 mRNA
2.0
1.5
1.0
0.5
0.0
*
*
miR-30e - + -
miR-NC1 - - +
B
HepG2-NTCP
IFNλ1 mRNA
15
10
5
0
**
**
HBV + + +
miR-30e - + +
miR-NC1 + - -
C
HeLa
IFNβ mRNA
100000
80000
60000
40000
20000
0
*** **
NDV - + + +
miR-30e - - + -
miR-NC1 - - - +
D
HeLa
CXCL10 mRNA
50
40
30
20
10
0
*** ***
NDV - + + +
miR-30e - - + -
miR-NC1 - - - +
E
HeLa
IL6 mRNA
80
60
40
20
0
*** ***
NDV - + + +
miR-30e - - + -
miR-NC1 - - - +
F
A549
IFIT1 mRNA
400
300
200
100
0
*** **
NDV - + + +
miR-30e - - + -
miR-NC1 - - - +
G
A549
CXCL10 pg/ml
300
200
100
0
*** ***
NDV - + + +
miR-30e - - + -
miR-NC1 - - - +
H
HeLa
CXCL10 pg/ml
600
400
200
0
*** ***
NDV - + + +
miR-30e - - + -
miR-NC1 - - - +
I
HeLa
IL6 pg/ml
400
300
200
100
0
*** ***
NDV - + + +
miR-30e - - + -
miR-NC1 - - - +
J
HEK293
Relative Luciferase Activity
100
80
60
40
20
0
*** ***
NDV - + + +
miR-30e - - + -
miR-NC1 - - - +
ISRE Promoter
K
HEK293
Relative Luciferase Activity
80
60
40
20
0
** **
NDV - + + +
miR-30e - - + -
miR-NC1 - - - +
IFNβ Promoter
L
HEK293
Relative Luciferase Activity
300
200
100
0
*** ***
NDV - + + +
miR-30e - - + -
miR-NC1 - - - +
NFκB Promoter

Figure S4 - miR-30e enhances innate immune responses during viral infection, Related to Figure 1. (A-F) Quantification of the fold changes in the relative abundances of indicated genes in the indicated cells measured by qRT-PCR after viral infection and transfection with/without miR-30e as described previously. (G-I) A549 and HeLa cells were mock transfected, transfected with miR-30e or miR-NC1 mimics and then infected with NDV (MOI 5), 24 hours after infection, the amounts of *CXCL10* and *IL6* protein secreted into the cell culture supernatant were measured by enzyme-linked immunosorbent assay (ELISA). (J-L) Quantification of ISRE/IFNβ/NFκB promoter activity by luciferase assay as indicated in HEK293 cells. Data are mean +/- SEM of triplicate samples from single experiment and are representative of two (A-B) and three (C-L) independent experiments. ***$P<0.001$, **$P<0.01$ and *$P<0.05$ by one-way ANOVA Tukey test.

Figure. S5

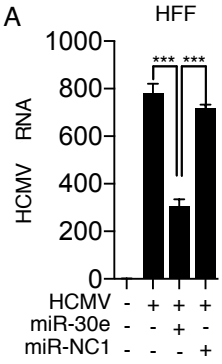
A
HFF
HCMV RNA
1000
800
600
400
200
0
***
***
HCMV - + + +
miR-30e - - + -
miR-NC1 - - - +

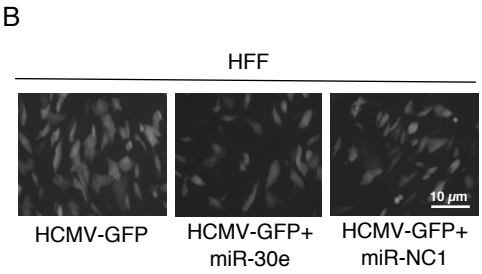
B
HFF
10 μm
HCMV-GFP
HCMV-GFP+ miR-30e
HCMV-GFP+ miR-NC1

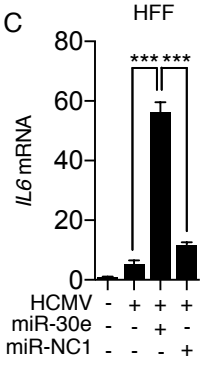
C
HFF
IL6 mRNA
80
60
40
20
0
***
***
HCMV - + + +
miR-30e - - + -
miR-NC1 - - - +

Figure S5 - miR-30e inhibits DNA virus replication, Related to Figure 1. HFF (Human foreskin fibroblast) cells were cultured in DMEM and transfected with miR-30e or miR-NC1 mimics then infected with HCMV-GFP virus (MOI = 5) and RNA were isolated to quantify the (A) HCMV transcript (Glycoprotein B) by using qRT-PCR and GFP signals (of HCMV-GFP tagged virus) by microscopy, (B) *IL6* transcript in indicated transfected miR-30e group compared with control miR-NC1. Data are mean +/- SEM of triplicate samples from single experiment and are representative of two independent experiments. ***$P<0.001$ and **$P<0.01$ by one-way ANOVA Tukey test.

Figure. S6

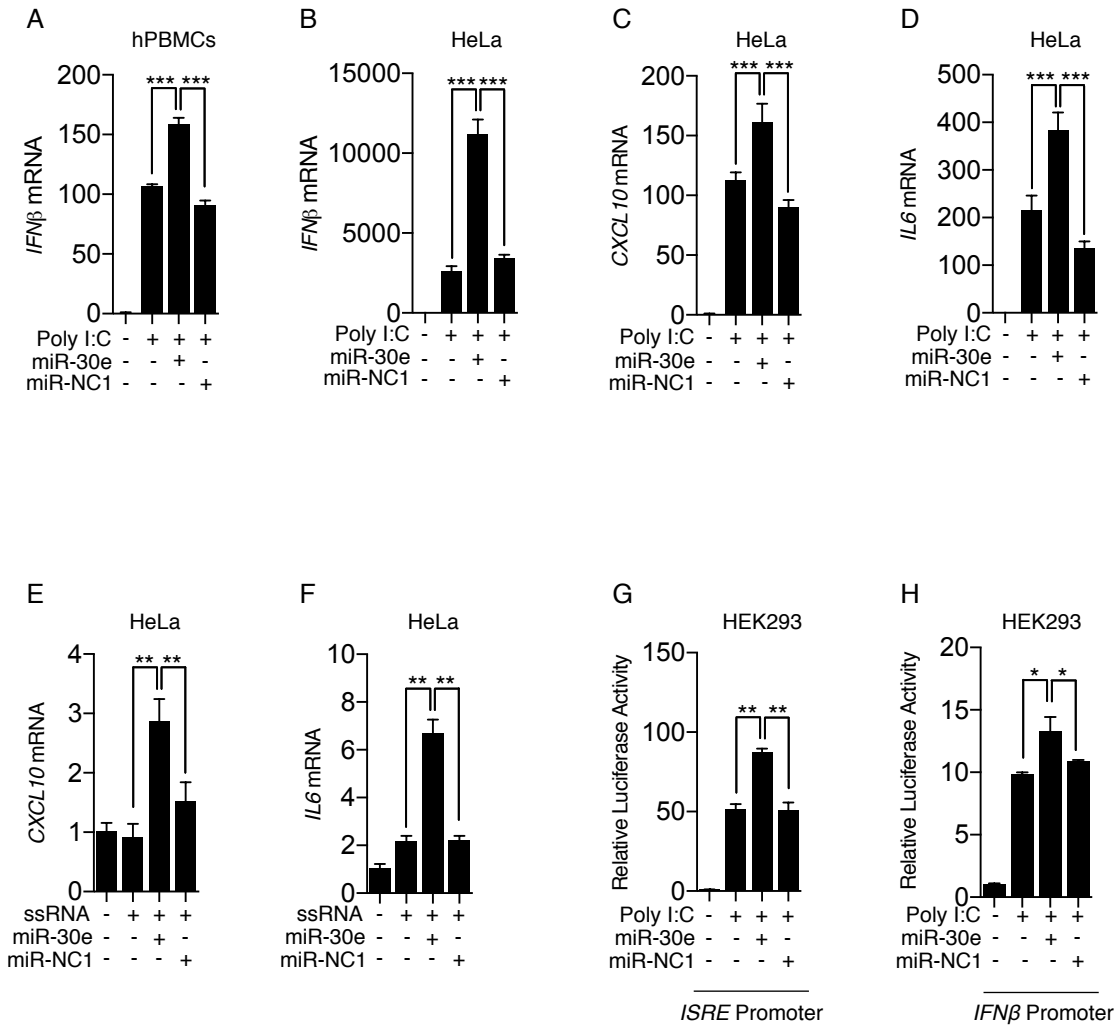
A
hPBMCs
IFNβ mRNA
200
150
100
50
0
***
***
Poly I:C - + + +
miR-30e - - + -
miR-NC1 - - - +
B
HeLa
IFNβ mRNA
15000
10000
5000
0
***
***
Poly I:C - + + +
miR-30e - - + -
miR-NC1 - - - +
C
HeLa
CXCL10 mRNA
200
150
100
50
0
***
***
Poly I:C - + + +
miR-30e - - + -
miR-NC1 - - - +
D
HeLa
IL6 mRNA
500
400
300
200
100
0
***
***
Poly I:C - + + +
miR-30e - - + -
miR-NC1 - - - +
E
HeLa
CXCL10 mRNA
4
3
2
1
0
**
**
ssRNA - + + +
miR-30e - - + -
miR-NC1 - - - +
F
HeLa
IL6 mRNA
10
8
6
4
2
0
**
**
ssRNA - + + +
miR-30e - - + -
miR-NC1 - - - +
G
HEK293
Relative Luciferase Activity
150
100
50
0
**
**
Poly I:C - + + +
miR-30e - - + -
miR-NC1 - - - +
ISRE Promoter
H
HEK293
Relative Luciferase Activity
20
15
10
5
0
*
*
Poly I:C - + + +
miR-30e - - + -
miR-NC1 - - - +
IFNβ Promoter

Figure S6 - miR-30e enhances innate immune responses upon viral PAMPs treatment, Related to Figure 1. (A-F) Quantification of indicated transcripts in indicated cells (measured by qRT-pCR) transfected with mir-30e or miR-NC1 for 24 hours and then treated with (A-D) poly IC (10μg/ml) and (E-F) ssRNA (2μg/ml) treatment respectively. (G, H) HEK 293T cells transfected with miR-30e (25 nM) or miR-NC1 (25 nM) mimics, pRL-TK (50 ng) and indicated luciferase reporters for ISRE/IFNβ (200 ng) then stimulated with poly IC for 24 hours. Cells were then lysed to analyze the promoter activity by luciferase assay. Data are mean +/- SEM of triplicate samples from single experiment and are representative of three independent experiments. ***$P<0.001$, **$P<0.01$ and *$P<0.05$ by one-way ANOVA Tukey test.

A

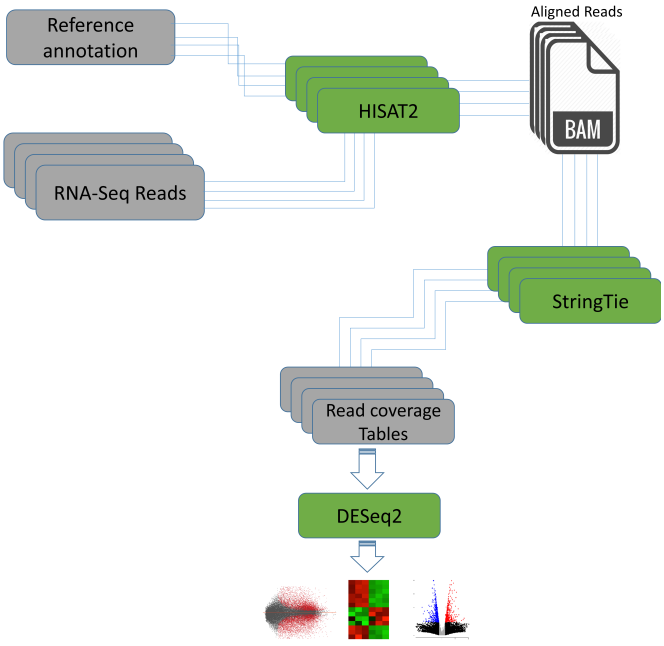

Representation of differentially expressed genes in plots and heat maps

C

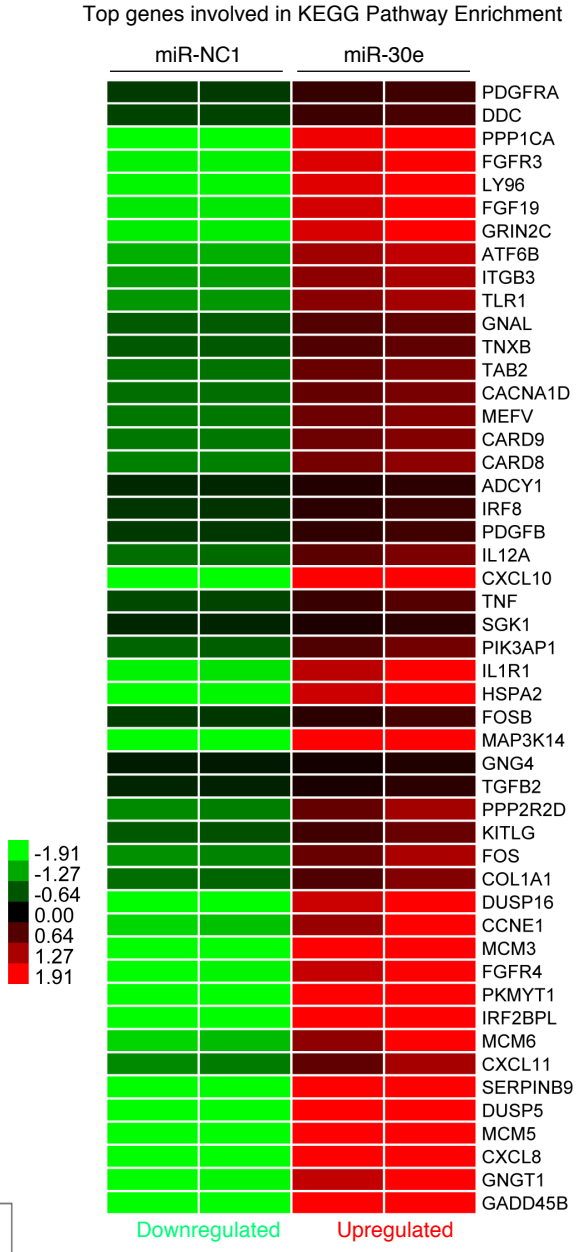

B

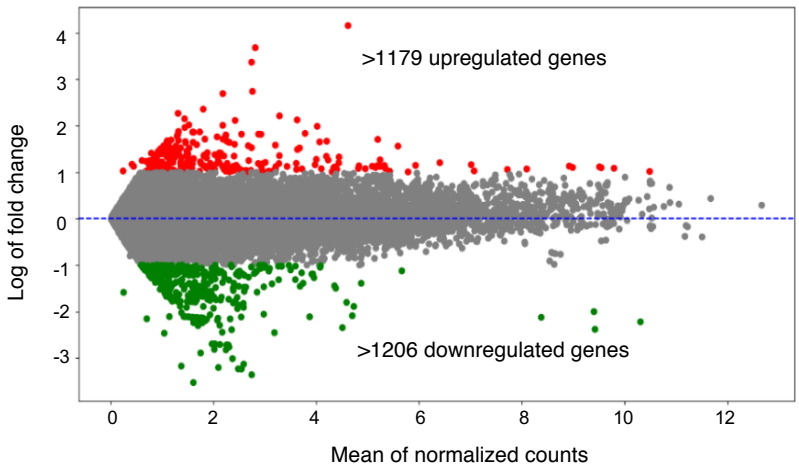

Figure S7 – miR-30e differentially expressed genes during NDV infection, Related to Figure 2. (A) Workflow for the analysis of RNA-Sequencing data from raw sequencing reads to expression profiles of differentially expressed genes represented through different plots and heat maps. (B) MA (M=log ratio and A=mean average) plot for differential expression of genes, indicating upregulated (in red) and downregulated (in green) genes. (C) Heat map representing relative abundance of genes involved in top enriched KEGG pathways in figure 2E.

Figure. S8

TRIM 38

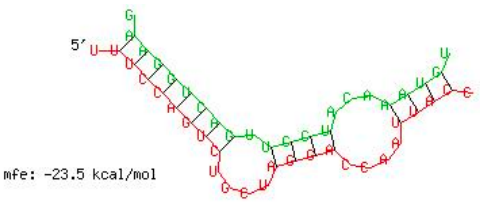

TRIM13

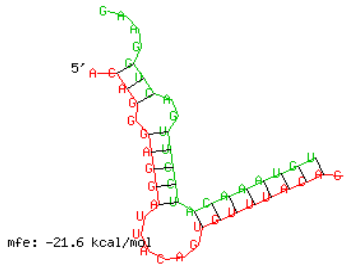

TANK

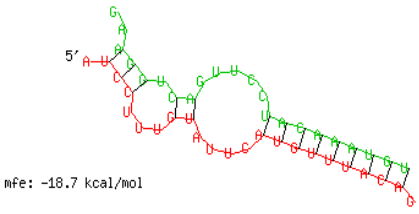

ATG 5

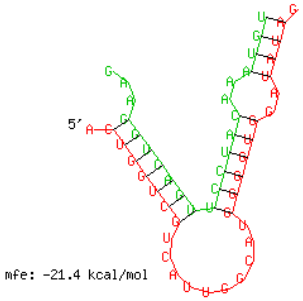

ATG 12

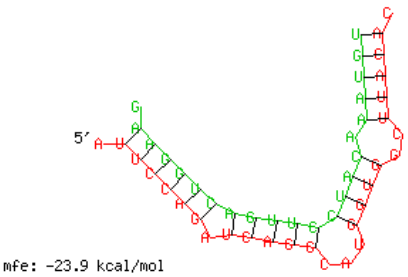

BECN1

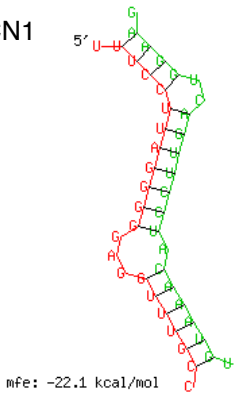

EPG5

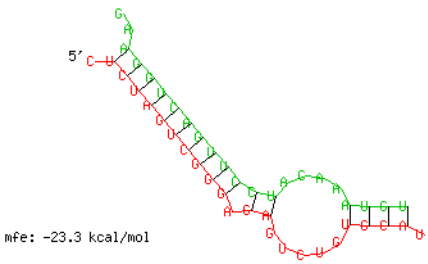

SOCS1

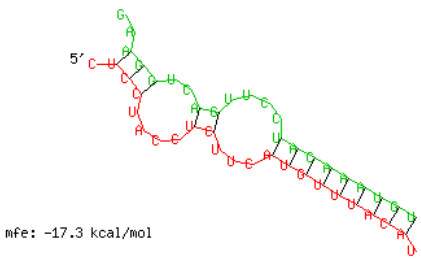

SOCS3

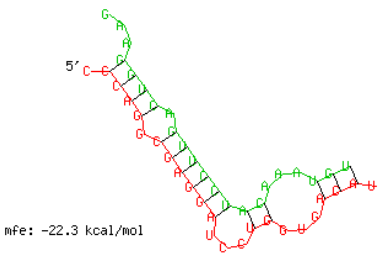

JAK1

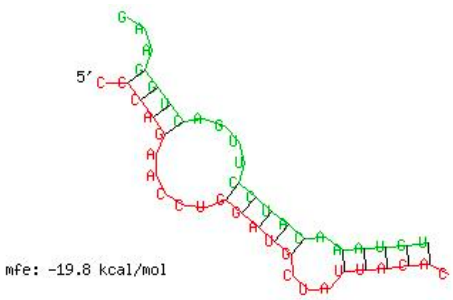

STAT1

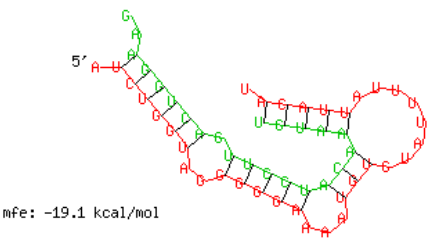

Figure S8 – Minimum free energy (mfe) for binding efficiency of miR-30e to negative regulators, Related to Figure 3. Representation of minimum free energy diagrams for negative regulators (*TRIM38, TRIM13, TANK, ATG5, ATG12, BECN1, EPG5, SOCS1* and *SOCS3*) and positive regulators (*JAK1* and *STAT1*) targeted by miR-30e.

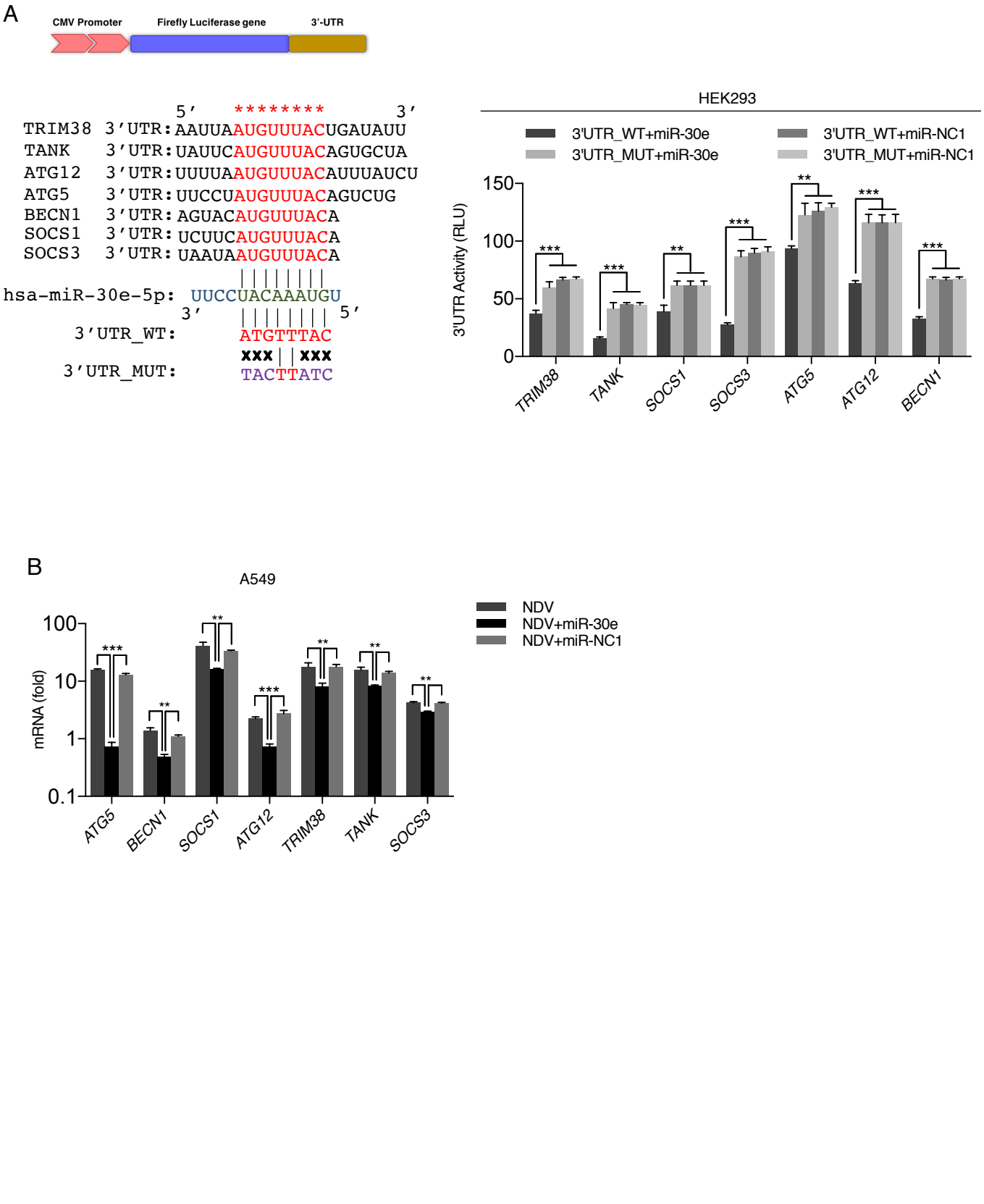
A
CMV Promoter
Firefly Luciferase gene
3'-UTR
5' ******** 3'
TRIM38 3'UTR: AAUUAAUGUUUACUGAUAUU
TANK 3'UTR: UAUUCAUGUUUACAGUGCUA
ATG12 3'UTR: UUUUAAUGUUUACAUUUAUCU
ATG5 3'UTR: UUCCUAUGUUUACAGUCUG
BECN1 3'UTR: AGUACAUGUUUACA
SOCS1 3'UTR: UCUUCAUGUUUACA
SOCS3 3'UTR: UAAUAAUGUUUACA
hsa-miR-30e-5p: UUCCUACAAAUGU
3' 5'
3'UTR_WT: ATGTTTAC
3'UTR_MUT: TACTTATC
HEK293
3'UTR_WT+miR-30e
3'UTR_MUT+miR-30e
3'UTR_WT+miR-NC1
3'UTR_MUT+miR-NC1
3'UTR Activity (RLU)
150
100
50
0
TRIM38
TANK
SOCS1
SOCS3
ATG5
ATG12
BECN1
B
A549
mRNA (fold)
100
10
1
0.1
ATG5
BECN1
SOCS1
ATG12
TRIM38
TANK
SOCS3
NDV
NDV+miR-30e
NDV+miR-NC1

Figure S9 – Quantification of innate immune negative regulators in presence of miR-30e, Related to Figure 3. (A) 3'-UTRs of all selected target genes having binding sites for seed sequence in miR-30e were conserved throughout (shown in red). HEK293 cells were transfected with miR-30e or miR-NC1 (25nM) mimic and 50 ng of pRL-TK along with 300ng of 3'UTR_WT or 300ng of 3'UTR_MUT for 24 hours, the cell was lysed and subjected to luciferase assay. (B) Quantification of the fold changes by qRT-PCR analysis in the relative abundances of negative regulator transcripts (*TRIM38, TANK, ATG5, ATG12, BECN1, SOCS1* and *SOCS3*) after infection of NDV (MOI = 5) for 24 hours in A549 cells prior to transfected with miR-30e or miR-NC1 as indicated. Data are mean +/- SEM of triplicate samples from single experiment and are representative of three independent experiments. ***$P<0.001$, **$P<0.01$ and *$P<0.05$ by one-way ANOVA Tukey test.

Figure. S10

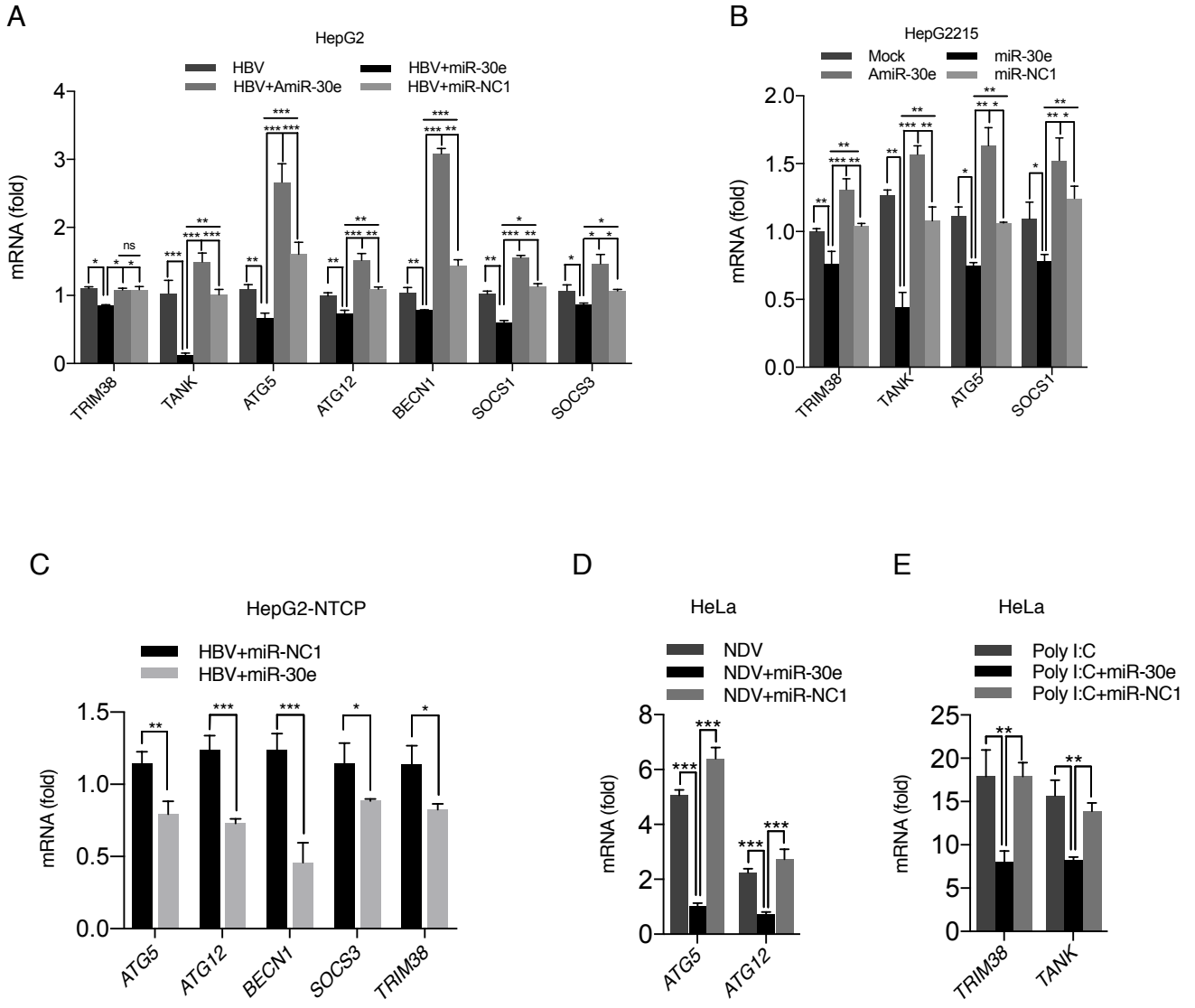
A
HepG2
HBV
HBV+AmiR-30e
HBV+miR-30e
HBV+miR-NC1
mRNA (fold)
TRIM38
TANK
ATG5
ATG12
BECN1
SOCS1
SOCS3
B
HepG2215
Mock
AmiR-30e
miR-30e
miR-NC1
mRNA (fold)
TRIM38
TANK
ATG5
SOCS1
C
HepG2-NTCP
HBV+miR-NC1
HBV+miR-30e
mRNA (fold)
ATG5
ATG12
BECN1
SOCS3
TRIM38
D
HeLa
NDV
NDV+miR-30e
NDV+miR-NC1
mRNA (fold)
ATG5
ATG12
E
HeLa
Poly I:C
Poly I:C+miR-30e
Poly I:C+miR-NC1
mRNA (fold)
TRIM38
TANK

Figure S10 – Quantification of innate immune negative regulators in presence of miR-30e, Related to Figure 3. (A-E) Quantification of the fold changes by qRT-PCR analysis in the relative abundances of negative regulator transcripts (*TRIM38, TANK, ATG5, ATG12, BECN1, SOCS1* and *SOCS3*) in (A) HepG2 cells remain untransfecd, transfected with miR-30e, AmiR-30e or miR-NC1 for 48 hours then treated with HBV-PS for HBV infection, (B) HepG2215 cells transfected as described previously, (C) HepG2-NTCP cells transfected with miR-30e and miR-NC1 for 48 hours then infected with HBV infection. (D-E) HeLa cells remain untransfecd, transfected with miR-30e or miR-NC1 for 24 hours then (D) infected with NDV (MOI = 5) or (E) treated with poly IC for 24 hours. Data are mean +/- SEM of triplicate samples from single experiment and are representative of two independent experiments. ***$P<0.001$, **$P<0.01$ and *$P<0.05$ by one-way ANOVA Tukey test.

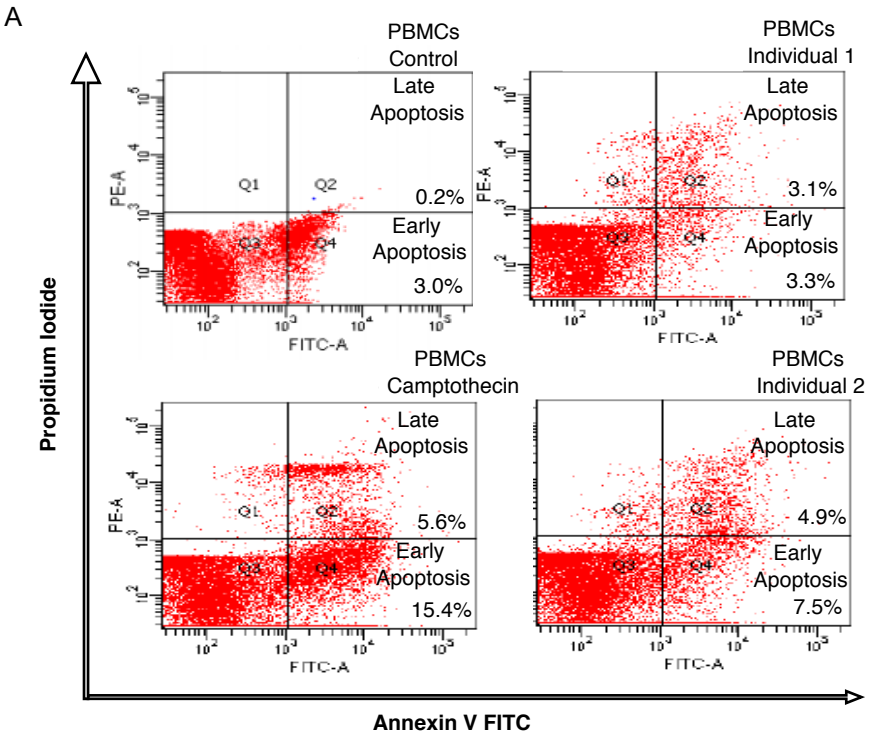
A
PBMCs
Control
Late
Apoptosis
0.2%
Early
Apoptosis
3.0%
PBMCs
Individual 1
Late
Apoptosis
3.1%
Early
Apoptosis
3.3%
PBMCs
Camptothecin
Late
Apoptosis
5.6%
Early
Apoptosis
15.4%
PBMCs
Individual 2
Late
Apoptosis
4.9%
Early
Apoptosis
7.5%
Q1
Q2
Q3
Q4
PE-A
FITC-A
Propidium Iodide
Annexin V FITC

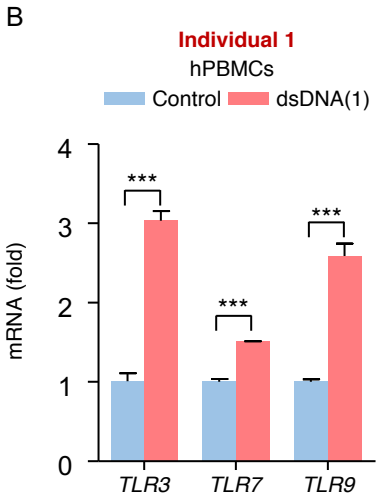
B
Individual 1
hPBMCs
Control
dsDNA(1)
mRNA (fold)
***
***
***
TLR3
TLR7
TLR9

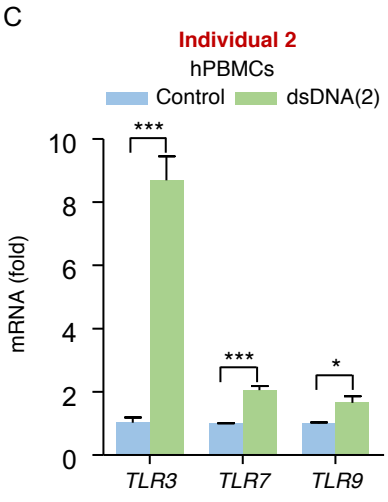
C
Individual 2
hPBMCs
Control
dsDNA(2)
mRNA (fold)
***
***
*
TLR3
TLR7
TLR9

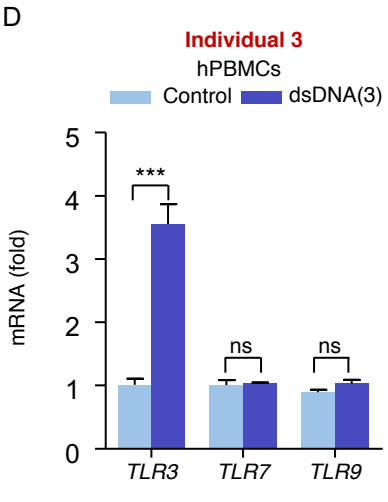
D
Individual 3
hPBMCs
Control
dsDNA(3)
mRNA (fold)
***
ns
ns
TLR3
TLR7
TLR9

Figure S11 – DAMP (ds DNA) induce apoptosis and TLR 3/7/9, Related to Figure 4.

(A) Human PBMCs remain untreated or treated with Camptothecin, dsDNA separately from two different individuals (as indicated 1 and 2) and subjected to Annexin PI assay to detect the apoptosis level within the PBMCs using flow cytometry. (B-D) Quantification of the fold changes by qRT-PCR analysis in the relative abundances of respective transcripts (*TLR3, TLR7* and *TLR9)* in all three individuals. Data are mean +/- SEM of triplicate samples from single experiment and are representative of three independent experiments. ***$P<0.001$ and **$P<0.01$ by paired t-test.

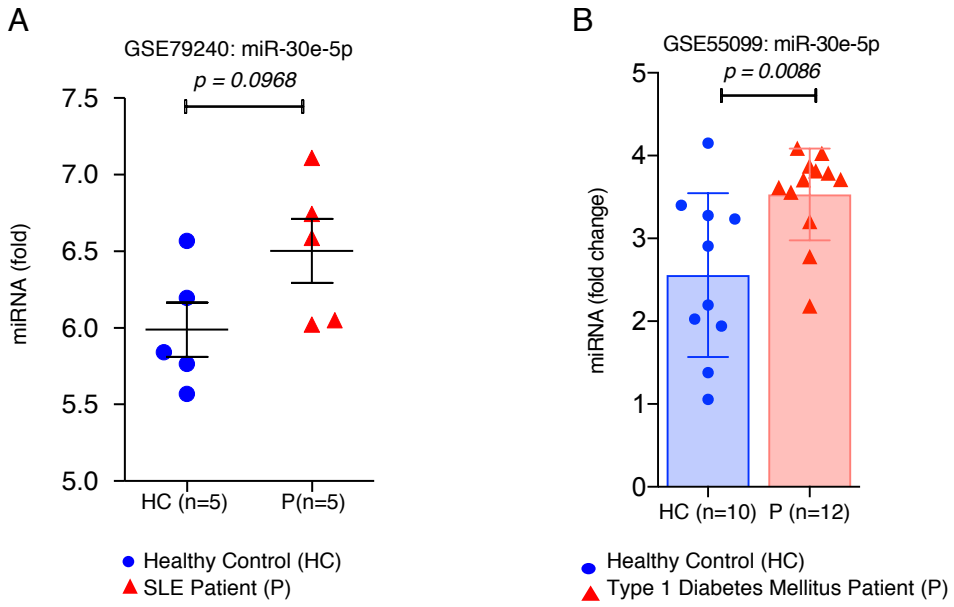
A
GSE79240: miR-30e-5p
p = 0.0968
miRNA (fold)
7.5
7.0
6.5
6.0
5.5
5.0
HC (n=5)
P(n=5)
Healthy Control (HC)
SLE Patient (P)
B
GSE55099: miR-30e-5p
p = 0.0086
miRNA (fold change)
5
4
3
2
1
0
HC (n=10)
P (n=12)
Healthy Control (HC)
Type 1 Diabetes Mellitus Patient (P)

Figure S12 – GEO Datasets re-analyzed to demonstrate the expression level of miR-30e in autoimmune disorder, Related to Figure 5. (A) SLE (GSE79240) - Non-coding RNA profiling by microarray in dendritic cells of SLE patients (P) compared to healthy controls (HC). Data points include fold change of miR-30e among 5 patients ($p = 0.0968$). (B) Type 1 Diabetes Mellitus (GSE55099) - Non-coding RNA profiling by microarray in PBMCs of patients (P) compared to healthy controls (HC). Data points include fold change of miR-30e among 12 patients compared to 10 healthy controls ($p = 0.0086$).

Figure. S13

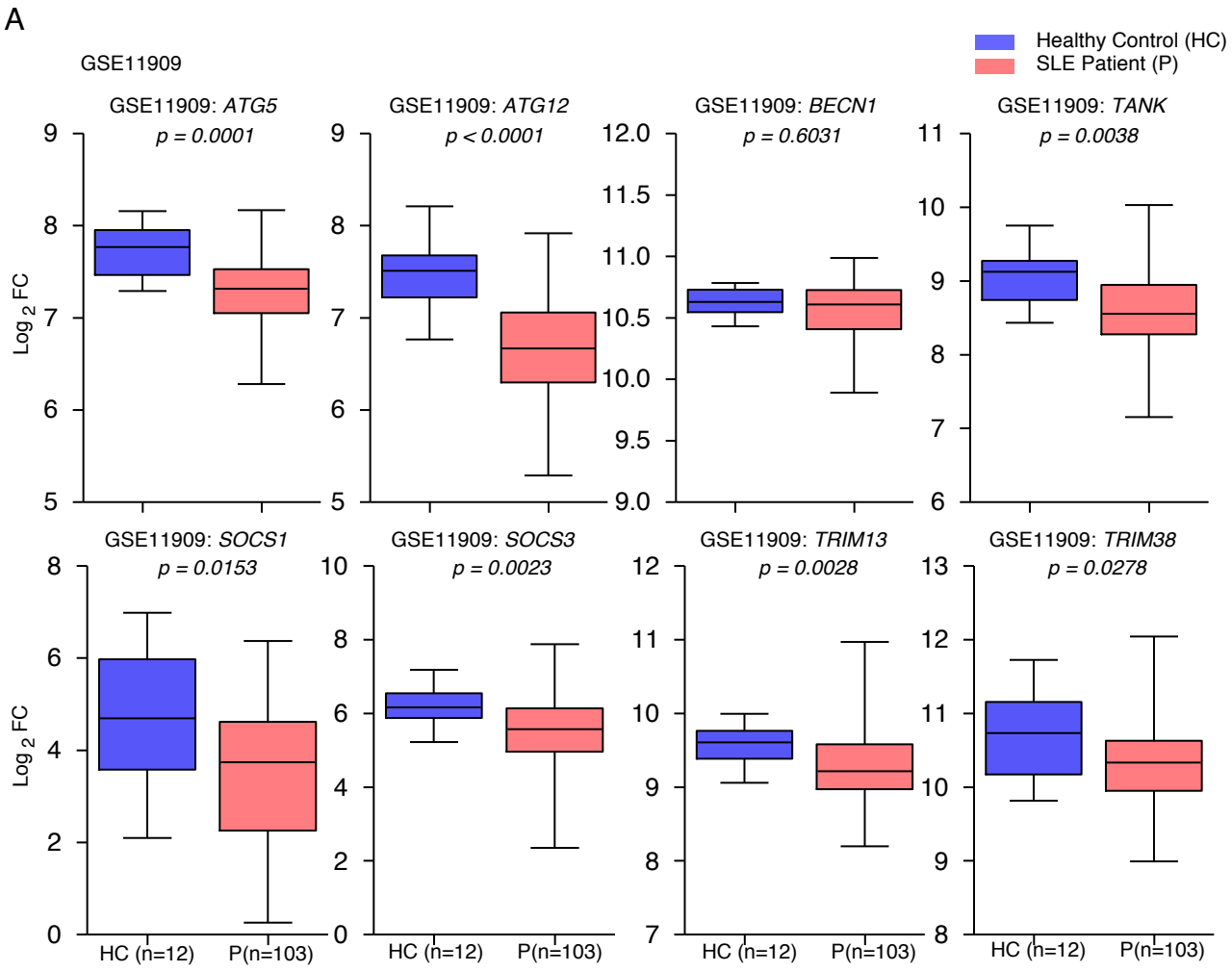
A
GSE11909
Healthy Control (HC)
SLE Patient (P)
GSE11909: ATG5
p = 0.0001
GSE11909: ATG12
p < 0.0001
GSE11909: BECN1
p = 0.6031
GSE11909: TANK
p = 0.0038
GSE11909: SOCS1
p = 0.0153
GSE11909: SOCS3
p = 0.0023
GSE11909: TRIM13
p = 0.0028
GSE11909: TRIM38
p = 0.0278
Log 2 FC
HC (n=12)
P(n=103)

Figure S13 – GEO Dataset-GSE11909 re-analyzed to demonstrate the transcript levels of innate negative regulators in SLE, Related to Figure 5. (A) Expression profiling by microarray to estimate the log fold change of following innate immune negative regulators during SLE pathogenesis in patients (P) compared to healthy controls (HC); *ATG5*, *ATG12*, *BECN1*, *TANK*, *SOCS1*, *SOCS3*, *TRIM13* and *TRIM38*.

A

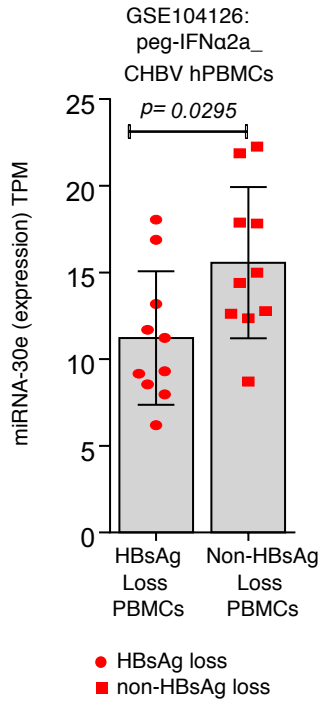
GSE104126:
peg-IFNα2a_
CHBV hPBMCs
p= 0.0295
miRNA-30e (expression) TPM
25
20
15
10
5
0
HBsAg Loss PBMCs
Non-HBsAg Loss PBMCs
HBsAg loss
non-HBsAg loss

Figure S14 – GEO Dataset-GSE104126 re-analyzed to demonstrate the expression level of miR-30e, Related to Figure 6. (A) Non-coding RNA profiling by microarray in PBMCs of two types of chronic hepatitis B (CHB) patients (HBsAg loss and non-HBsAg loss) after treatment with pegylated interferon (peg-IFNα2a). Data points include fold change of miR-30e among 10 patients ($p = 0.0295$).

	Therapy naive CHB (n=51)	Control (n=24)	*p-value*
Median age (range)	48(19-68)	31(23-55)	
Male/Female	36/15	10/14	
AST (reference range: 10 - 40 U/L)	37(18-166)	24(16-42)	
ALT (reference range:7-56U/L)	36(15-130)	23.5(12-48)	
HBsAg	Positive	Negative	
Anti-HBcIgM	Negative	…….	
HbeAg	16 positive	…….	
HBV DNA Load log10 (IU/mL)	5.03(1.36-9.2)	…….	
hsa-miR-30e-5p (fold change/U6)	18.2(0.63-269.12)	1.01(0.712-1.92)	0.0023***

Table T1: Demographic data of chronic hepatitis B (CHB) cohort and controls, Related to Figure 1. Data expressed as median (range); CHB (Chronic Hepatitis B); AST (aspartate transaminase); ALT (alanine transaminase); HBsAg (Hepatitis B surface Antigen); Anti-HBcIgM (IgM antibody to hepatitis B core antigen); HBeAg (Hepatitis B e-Antigen); hsa-miR-30e-5p (Human Micro(mi)-RNA-30e).

Negative Regulator	hsa-miR-30e Binding site	miRanda	DIANA	Target Scan	miRDB
TLR pathway		miRSVR Score	Pred.Score	Context++ Score	Target Score
TRIM 38	one site: 1157	-1.0306	---	-0.13	---
TANK	one site: 238	-1.0396	---	-0.29(highly conserved)	---
TRIM 35 [35]	one site: 281	-0.5210	0.756	-0.07	---
RIGI/MDA5 pathway					
ATG5	one site at:511	-1.2012	---	-0.44(highly conserved)	88
ATG12	two sites: 370, 388	-1.029 & -0.4650	Low score	-0.39	98
TRIM 13 [36]	two sites: 2740,3856	-0.1131 & -0.4454	---	---	64
TRIM 38	one site: 1157	-1.0306	---	-0.13	---
SOCS1	one site at:271	-1.2111	1.000	---	78
SOCS3	one site at:1411	-1.2147	0.998	---	85
BECN1	one site at:84	-1.3155	0.863	---	88
Inflammatory pathway/ Virus Reserves or Reactivation pathway					
EPG5 [37]	one site at:24	-0.4449	0.984	-0.25(highly conserved)	---
BECN 1	one site at:84	-1.3155	0.863	---	88
ATG5	one site at:511	-1.2012	---	-0.44(highly conserved)	88
DNA sensing pathway					
BECN1	one site at:84	-1.3155	0.863	---	88

Table T2 - *In-silico* analysis of miR-30e targets using indicated algorithms , Related to Figure 3.

TRIM 38

- Gene ID:ENSG00000112343
- Gene Name: TRIM38
- RBP:AGO2
- Sample ID:GSE44404-GSM1084065
- Method: HITS-CLIP
- Chromosome:chr6
- Strand :+
- Binding site start:25974460
- Binding site end:25974480
- Binding signal:14
- P-value:0.00319213
- Genomic position: intron

TANK

- Gene ID:ENSG00000136560
- Gene Name: TANK
- RBP:AGO2
- Sample ID:GSE41437-GSM1020022
- Method: PAR-CLIP
- Chromosome:chr2
- Strand :+
- Binding site start:162092600
- Binding site end:162092620
- Binding signal:22
- P-value:8.88536e-07
- Genomic position:3'UTR

ATG 5

- Gene ID:ENSG00000057663
- Gene Name: ATG5
- RBP:AGO2
- Sample ID:GSE44404-GSM1084068
- Method: HITS-CLIP
- Chromosome:chr6
- Strand : -
- Binding site start:106632780
- Binding site end:106632800
- Binding signal:15
- P-value:0.00079613
- Genomic position:3'UTR

ATG 12

- Gene ID:ENSG00000145782
- Gene Name: ATG12
- RBP:AGO2
- Sample ID:GSE42701-GSM1048187
- Method: HITS-CLIP
- Chromosome:chr5
- Strand :-
- Binding site start:115167220
- Binding site end:115167240
- Binding signal:18
- P-value:0.00794433
- Genomic position:3'UTR

BECN1

- Gene ID:ENSG00000126581
- Gene Name: BECN1
- RBP:AGO2
- Sample ID:GSE28865-GSM714644
- Method: PAR-CLIP
- Chromosome:chr17
- Strand :-
- Binding site start:40962420
- Binding site end:40962440
- Binding signal:29
- P-value:2.98304e-08
- Genomic position:3'UTR

SOCS1

- Gene ID:ENSG00000185338
- Gene Name: SOCS1
- RBP:AGO2
- Sample ID:GSE28865-GSM714644
- Method: PAR-CLIP
- Chromosome:chr16
- Strand :-
- Binding site start:11348400
- Binding site end:11348420
- Binding signal:25
- P-value:2.5004e-07
- Genomic position:3'UTR

SOCS3

- Gene ID:ENSG00000184557
- Gene Name: SOCS3
- RBP:AGO2
- Sample ID:GSE42701-GSM1048188
- Method: HITS-CLIP
- Chromosome:chr17
- Strand :-
- Binding site start:76352920
- Binding site end:76352940
- Binding signal:62
- P-value:4.01318e-06
- Genomic position:3'UTR

TRIM13

- Gene ID:ENSG00000204977
- Gene Name: TRIM13
- RBP:AGO2
- Sample ID:GSE44404-GSM1084044
- Method: HITS-CLIP
- Chromosome:chr13
- Strand :+
- Binding site start:50591100
- Binding site end:50591120
- Binding signal:9
- P-value:0.00312875
- Genomic position: 3'UTR

EPG5

- Gene ID:ENSG00000152223
- Gene Name: EPG5
- RBP:AGO2
- Sample ID:GSE44404-GSM1084047
- Method: HITS-CLIP
- Chromosome:chr18
- Strand :-
- Binding site start:43432360
- Binding site end:43432380
- Binding signal:9
- P-value:0.000552801
- Genomic position:3'UTR

Table T3 - CLIP database analysis for miR-30e targets , Related to Figure 3.

S. No.	Age	Gender	Duration of disease (years)	Disease activity (SLEDAI)	Drugs	Serum complement level	Anti-nuclear antibody	Anti-dsDNA (IU)	Major oragn involved
1	23	Female	7	20	Pred, HCQS,	Low	Positive	212.3	Nephritis, gangrene
2	26	Female	5	24	Pred, HCQS	Low	Positive	>300	Nephritis
3	10	Female	0.3	6	Pred, HCQS	Low	Positive	>300	None
4	29	Female	7	2	Pred, HCQs,	Normal	Positive	>300	Interstitial lung disease
5	35	Female	0.5	13	Pred, HCQs, Thyroxin	low	Positive	>300	Nephritis, hemolytic anemia
6	25	Female	3	12	Pred, HCQS,	low	Positive	>300	Nephritis with renal failure
7	32	Female	4	8	Pred, HCQS,	Low	Positive	>300	Nephritis
8	27	Female	0.45	25	Pred, HCQs,	Low	Positive	>300	Nephritis
9	33	Female	8	0	Pred	not available	Positive	<10	Momoneuritis
10	20	Female	1	8	Pred, HCQS,	Low	Positive	88.6	Nephritis
11.	55	Female	7	12	Pred, HCQS,	Low	Positive	>300	Nephritis
12.	40	Female	0.5	6	Pred, MMF, Tac, HCQS	Low	Positive	130.2	Nephritis
13.	22	Female	6	4	none	Low	Positive	<10	None

Table T4 - SLE patients details used in the study, Related to Figure 5.

Pred: Prednisolone, MMF: Mycophenolate mofetil, Tac: Tacrolimus, HCQS: Hydroxychloroquine

	Baseline (n=7)	Post-treatment (n=7)	*p-value*
Median age (range)	32(23-60)	-	
Male	7	-	
AST (reference range: 10 - 40 U/L)	48.28(24.02-111.31)	41.57(25.28-91.2)	
ALT (reference range:7-56U/L)	27.27(19-47.6)	21.81(16.36-57.27)	
HbeAg	4 positive	4 positive	
HBV DNA Load log10 (IU/mL)	6.55(3.5-7.56)	3.2(1.28-3.94)	
hsa-miR-30e-5p (fold change/U6)	1.179(0.83-1.42)	0.199(0.046-1.34)	0.0313*

Table T5 - Demographic data of chronic hepatitis B (CHB) patients after Peg-interferon treatment, Related to Figure 6. Data expressed as median (range); Baseline (before treatment); AST (aspartate transaminase); ALT (alanine transaminase); HBsAg (Hepatitis B surface Antigen); Anti-HBcIgM (IgM antibody to hepatitis B core antigen); HBeAg (Hepatitis B e-Antigen); hsa-miR-30e-5p (Human Micro(mi)-RNA-30e).

Real Time PCR primers

	5'-----sequence-----3'
18S_Fw	CTGCTTTCCTCAACACCACA
18S_Rv	ATCCCTGAAAAGTTCCAGCA
HBV RNA_Fw	GCACTTCGCTTCACCTCTGC
HBV RNA_Rv	CTCAAGGTCGGTCGTTGACA
HBVcccDNA_Fw	GGACTTGAATGTACGTTGGGG
HBVcccDNA_Rv	GGACTTGAATGTACGTTGGG
HBV DNA_Fw	ATGGAGAACACAACATCAGG
HBV DNA_RV	GAGGCATAGCAGCAGGATG
NDV_Fw	GGAGGATGTTGGCAGCATT
NDV_Rv	GTCAACATATACACCTCATC
SeV_Fw	CAGAGGAGCACAGTCTCAGTGTTC
SeV_Rv	TCTCTGAGAGTGCTGCTTATCTGTGT
HCMV_GLYB_Fw	AAGTACCCCTATCGCGTGTG
HCMV_GLYB_Rv	ATGATGCCCTCATCCAAGTC
IFIT1_Fw	TCAGGTCAAGGATAGTCTGGAG
IFIT1_Rv	AGGTTGTGTATTCCCACACTGTA
IFNa_Fw	TGCTTTACTGATGGTCCTGGT
IFNa_Rv	TCATGTCTGTCCATCAGACAG
IFNb_Fw	AGCTGCAGCAGTTCCAGAAG
IFNb_Rv	AGTCTCATTCCAGCCAGTGC
IFNλ1_Fw	CGCCTTGGAAGAGTCACTCA
IFNλ1_Rv	GAAGCCTCAGGTCCCAATTC
IL6_Fw	CTCAGCCCTGAGAAAGGAGA
IL6_Rv	CCAGGCAAGTCTCCTCATTG
OAS1_Fw	GAGCTCCAGGGCATACTGAG
OAS1_Rv	CCAAGCTCAAGAGCCTCATC
IP10_Fw	TGGCATTCAAGGAGGTACCTCTC
IP10_Rv	TGATCTCAACACGTGGACAAA
TLR-3_Fw	TTGCCTTGTATCTACTTTTGGGG
TLR-3_Rv	TCAACACTGTTATATTTGTGGGT
TLR-7_Fw	TCAAGCCTTAGATTGGCGATGTC
TLR-7_Rv	CCAGATTGATTTGGGAATTTGTG
TLR-9_Fw	AGTCCTCGACCTGGCAGGAA
TLR-9_Rv	GCGTTGGCGCTAAGGTTGA
miR_30e_5p_Prom_Fw	CGCGGTACCCTTAACTATACTAAATATGTTGGG
miR_30e_5p_Prom_Rv	CGCAAGCTTGTAGCAAAGACTGCCCAGAAAG
mIL6_Fw	CCTCTGGTCTTCTGGAGTACC
mIL6_Rv	ACTCCTTCTGTGACTCCAGC
mIP10_Fw	ACCATGAACCCAAGTGCTG
mIP10_Rv	GTGGCAATGATCTCAACACG
mTNFa_Fw	ATGAGCACAGAAAGCATGA
mTNFa_Rv	AGTAGACAGAAGAGCGTGGT
NPM1_Fw	GATCTCTGGCAGTGGAGGAA
NPM1_Rv	CAAGCAAAGGGTGGAGTTCC
ATG5_Fw	ACTAGTGACCAGAAACACTTCGCTGC
ATG5_Rv	ACGCGTTTCCTCTAGGGCATTGTAGGC
ATG12_Fw	TTCCAACTTCTTGGTCTGGG
ATG12_Rv	AGAAGTGGGCAGTAGAGCGA
BECN1_Fw	TGTCTCTCGCAGATTCATCC
BECN1_Rv	ACGTTGAGCTGAGTGTCCAG
SOCS1_Fw	CACATGGTTCCAGGCAAGTA
SOCS1_Rv	CTACCTGAGCTCCTTCCCCT
SOCS3_Fw	TCCCCCCAGAAGAGAGCCTATTAC
SOCS3_Rv	TCCGACAGAGATGCTGAACCATCC
TANK_Fw	CCTCTTCGTCCTGTAGCATCA
TANK_Rv	GCATTGTTAGAGCCTGTGGA
TRIM38_Fw	GAAGACGTATGCCAGGGCTAC
TRIM38_Rv	GGAGATTCTTAAAGTCAGACCGG
m18S_Fw	GTAACCCGTTGAACCCCATT
m18S_Rv	CCATCCAATCGGTAGTAGCG
matg5_Fw	GACAAAGATGTGCTTCGAGATGTG
matg5_Rv	GTAGCTCAGATGCTCGCTCAG
matg12_ Fw	TGGCCTCGGAACAGTTGTTTA
matg12 _Rv	GGGCAAAGGACTGATTCACAT
msocs1_Fw	TCCGATTACCGGCGCATCACG
msocs1_Rv	CTCCAGCAGCTCGAAAAGGCA
msocs3_Fw	CACAGCAAGTTTCCCGCCGCC
msocs3_Rv	GTGCACCAGCTTGAGTACACA

Cloning Primers (5'----sequence-----3')

ATG5_UTR_Spe_Fw	ATAAACTAGTGACCAGAAACACTTCGCTGC
ATG5_UTR_MluI_Rv	ATAAACGCGTTTCCTCTAGGGCATTGTAGGC
ATG5_UTR_SDM_Fw	AATGACTTTGATAATGAACAGTGAG
ATG5_UTR_SDM_Rv	TGTAGTTAAGGAAAGATGGGTTTAC
ATG12_UTR_Spe_Fw	ATAAACTAGTCACGGAAGAGACAGCTCTGA
ATG12_UTR_HindIII_Rv	ATAAAAGCTTGGCACTCAATATGTGAATGACAG
BECN1_UTR_Fw_SpeI	ACTAGTGGGAGGTTTGCCTTAAAGGC
BECN1_UTR_Rv_MluI	ACGCGTGGCAGTTTTCAGACTGCAGC
BECN1_UTR_SDM_Fw	AATAAGAAAAAATCCACAAAAGC
BECN1_UTR_SDM_Rv	TGTATACCCGAATTTAATTTAAAACATG
SOCS1_UTR_HindIII_Fw	AAGCTTGATGGTAGCACACAACCAGGTG
SOCS1_UTR_SalI_Rv	GTCGACTAAAGCCAGACCCTCCC
SOCS1_UTR_SDM_Fw	TATGCTTTGCACAAACCAGGGG
SOCS1_UTR_SDM_Rv	AGTATAGGAGGTGCGAGTTCAG
SOCS3_UTR_SpeI_Fw	ACTAGTAAGGGCGCAAAGGGCAT
SOCS3_UTR_HindIII_Rv	AAGTTTAGCCTCAAGGGCCTGAG
SOCS3_UTR_SDM_Fw	TATGTCACTCTGTCTTTTATAAAGATTC
SOCS3_UTR_SDM_Rv	AGTAGAAACAAACAAAAAAATAGAGAAAAAAAC
TANK_UTR_Fw_SpeI	ACTAGTGACATTTGAAAACAGACATATCAAG
TANK_UTR_Rv_HindIII	AAGCTTGACACATTTGAAAACAGACATATCAAG
TANK_UTR_SDM_Fw	TATGTAATTCAAAATTATGTATGTGACTTAG
TANK_UTR_SDM_Rv	AGTAATTACAGTTTTATACAGAATTTTTTTTG
TRIM38_UTR_Spe_Fw	ACTAGTGATGGGGGATTCAGTTCTGG
TRIM38_UTR_HindIII_Rv	AAGCTTGTCTGGGTCAGCATACCGAG
TRIM38_UTR_SDM_Fw	TTAAACAAATCTGATATTTGTTGAAGTCCTAC
TRIM38_UTR_SDM_Rv	TCAGATTTGTTTAATTTTTTTTTTCCTTGAGGCAC

Table T6: List of primers used in the study, Related to Figure 1-6

Supplementary Information - Full Blot Images of Western Blot Analysis (shown in Figure 3F), Related to Figure 3

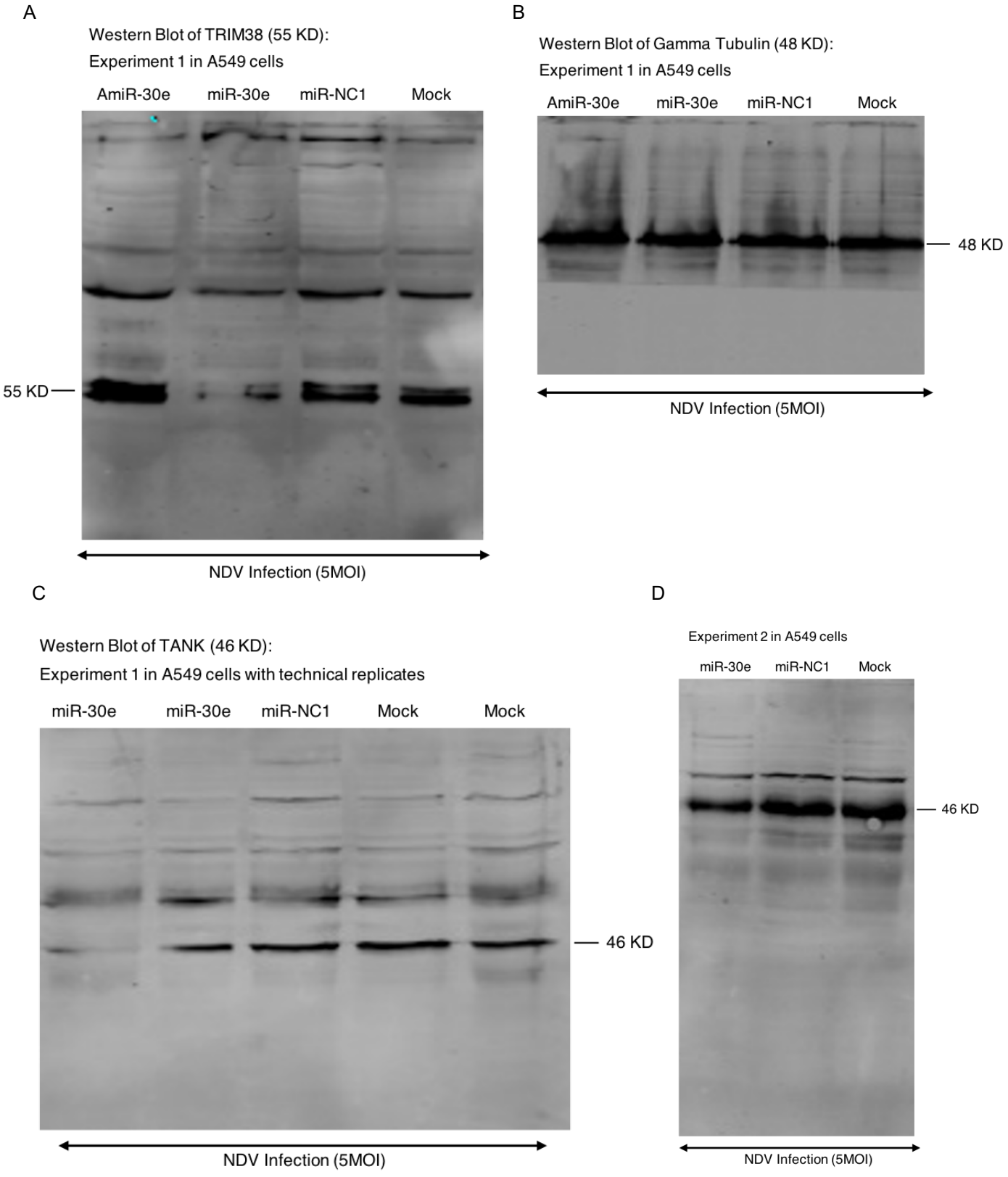

A

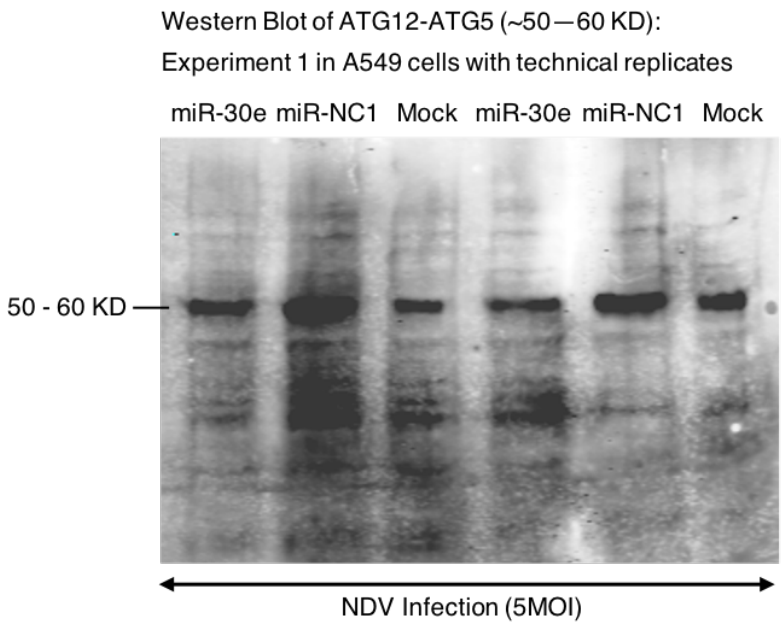
Western Blot of ATG12-ATG5 (~50—60 KD):
Experiment 1 in A549 cells with technical replicates
miR-30e miR-NC1 Mock miR-30e miR-NC1 Mock
50 - 60 KD
NDV Infection (5MOI)

B

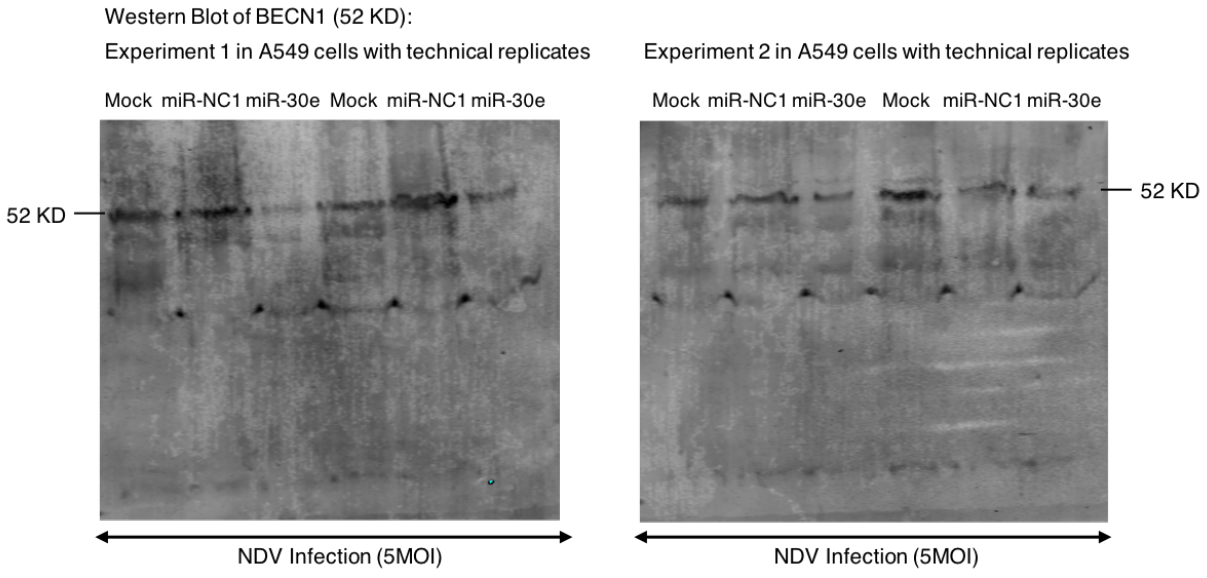
Western Blot of BECN1 (52 KD):
Experiment 1 in A549 cells with technical replicates
Mock miR-NC1 miR-30e Mock miR-NC1 miR-30e
52 KD
NDV Infection (5MOI)
Experiment 2 in A549 cells with technical replicates
Mock miR-NC1 miR-30e Mock miR-NC1 miR-30e
52 KD
NDV Infection (5MOI)

A

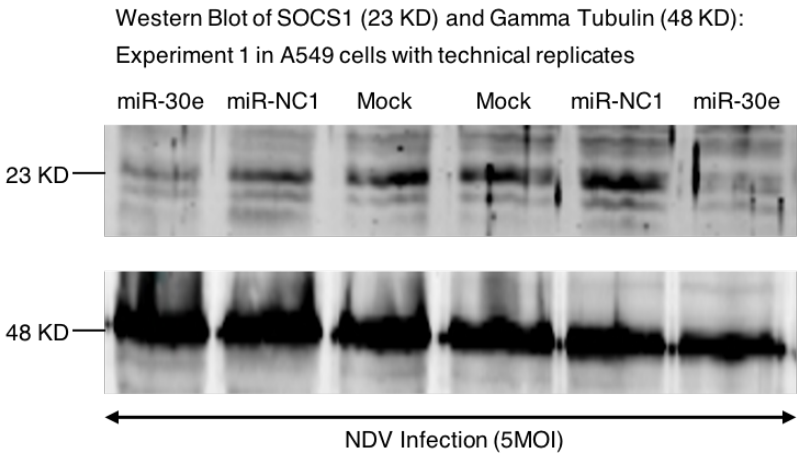
Western Blot of SOCS1 (23 KD) and Gamma Tubulin (48 KD):
Experiment 1 in A549 cells with technical replicates
miR-30e
miR-NC1
Mock
Mock
miR-NC1
miR-30e
23 KD
48 KD
NDV Infection (5MOI)

B

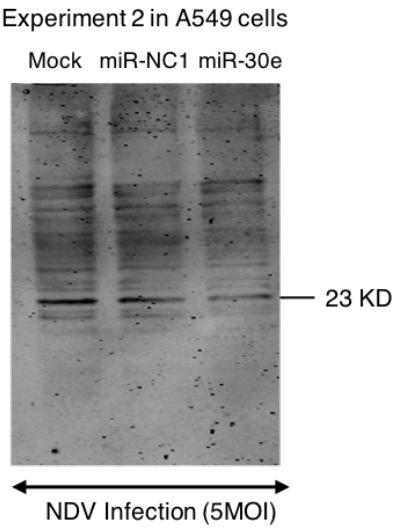
Experiment 2 in A549 cells
Mock
miR-NC1
miR-30e
23 KD
NDV Infection (5MOI)

C

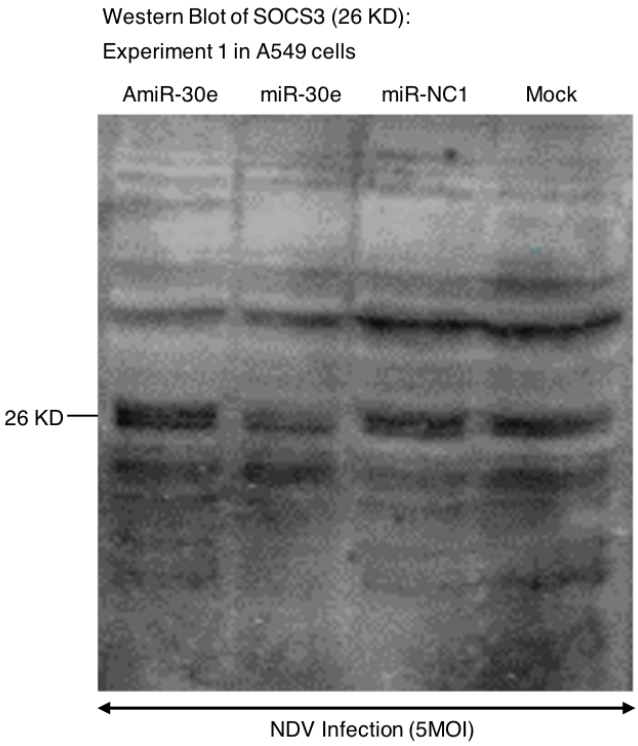
Western Blot of SOCS3 (26 KD):
Experiment 1 in A549 cells
AmiR-30e
miR-30e
miR-NC1
Mock
26 KD
NDV Infection (5MOI)

Transparent Methods

Ethical Statement. Experiments were performed after approval from the Institutional Ethical Committee (IEC)-Indian Institute of Science Education and Research (IISER) Bhopal: (IISERB/IEC/Certificate/20l6-IV/03), Institute Biosafety Committee (IBSC) - IISER-Bhopal: (IBSC/IISERB/2018/Meeting II/08), Bhopal Memorial Hospital & Research Centre Institutional Ethical Committee (IEC), BMHRC Research Projects/Clinical Studies (IRB/18/Research/10), Institutional Animal Ethical Committee (IAEC)-Small and Experimental Animal Facility National Institute of Immunology (NII): (IAEC#469/18) and Institutional Ethical Committee (IEC)- Sanjay Gandhi Post Graduate Institute of Medical Sciences (SGPGIMS): (2016-138-EMO-93).

Human blood samples. Blood samples from both healthy individuals and patients (HBV and SLE) were collected according to the ethics protocol in the respective hospitals by health professionals. Written informed consent was obtained from all patients and healthy participants before inclusion into the study at Bhopal Memorial Hospital & Research Center (BMHRC: for HBV samples: n = 51 Vs control samples: n = 24), Sanjay Gandhi Post Graduate Institute of Medical Sciences (SGPGIMS: for SLE samples: n = 13 Vs control samples: n = 13) and Institutional Ethical Committee (IEC)-Indian Institute of Science Education and Research (IISER) Bhopal. Reagents used for transfection/electroporation were Lipofectamine 2000, miRNA mimics, miRNA inhibitors, controls mimic/inhibitors and for RNA isolation were Trizol/Trizol-LS. All reagents used were procured from Ambion/Invitogen.

Mice. Systemic Lupus Erythematous (SLE) mouse model were procured from the Jackson Laboratory, USA and further breeding was done in approved pathogen- free, small animal facility

of National Institute of Immunology (NII). SLE mouse strains were used as follows: New Zealand White (NZW) and New Zealand Black (NZB) non-lupus bearing parent mice crossed to generate NZW/B F1 progenies, lupus induced mice. All the mice used in the study were from 6 to 12 weeks without any gender's bias. Dendritic cell enriched low density fraction of splenocytes were prepared as described earlier (Aliberti et al., 2003, Tamura et al., 2005). Spleens were harvested and single cell suspension of splenocytes were cultured in RPMI based media containing either 50nM of miR-30e antagomir and miR-NC1 antagomir (transfected through RNAimax transfecting reagent) and plated in 24-well plate (3 x 10^6 cells/well) maintained at 37ºC+5% CO_2. For the *in-vivo* experiments, four- 6 to 12 weeks old NZW/B F1 mice were randomly assigned into two groups. The mice in each group received four consecutives intravenous (retro-orbital) injections of either LNA antimiR-30e or LNA negative control (scrambled) compounds, formulated in TE Buffer (10mM Tris (pH: 7.5), 0.01mM EDTA) as per 25 mg LNA/kg mouse body weight on consecutive days as described previously. The mice were sacrificed within 24 h after the last dose. At selected time points, cells were harvested and relative abundances of miR-30e and other transcripts were quantified using qRT-PCR.

Cell lines, virus infections, transfection and reagents. A549 human alveolar basal epithelial cells (Cell Repository, NCCS, India), HEK293T/HEK293 human embryonic kidney cells (ATCC CRL-3216), Raw 264.7 (Cell Repository, NCCS, India), HeLa cervical cancer cells (Cell Repository, NCCS, India), HepG2-NTCP cells (from Dr. Takaji Wakita National Institute of Infectious Diseases Tokyo, Japan), HepG2 hepatoblastoma cells (from Dr. Nirupma Trehanpati's Laboratory, Institute of Liver & Biliary Sciences ILBS, New Delhi, India), HepG2215, HBV stably expressing hepatoblastoma cells (from Dr. Senthil Kumar Venugopal's Lab, South Asian

University, New Delhi, India) and HFFs (from Professor. Wade Gibson's Lab, Johns Hopkins, School of Medicine) were cultured in Dulbecco's modified Eagle's medium (DMEM) supplemented with 10% fetal bovine serum (FBS) and 1% Antibiotic-Antimycotic solution. HepG2-NTCP cells (from Dr. Takaji Wakita, National Institute of Infectious Diseases Tokyo, Japan). HepG2-NTCP cells were infected with HBV in Professor Akinori Takaoka's Laoboratoy as per the standard protocol (Sato et al., 2015) . Human PBMCs were isolated from whole blood and NDV LaSota viral stocks were accumulated as described previously (Ingle et al., 2015) . NDV-GFP was a kind gift from Professor Peter Palese, Icahn School of Medicine at Mount Sinai. Sendai-RFP (SeV-RFP) were provided by Dr. Sunil Raghav, ILS, Bhubaneshwar, India, A single virus stock was used for all experiments. The cells were infected in serum-free DMEM with the NDV and SeV viruses at the MOIs indicated in the figure legends. After 60 min, the cells were washed with phosphate-buffered saline (PBS) and then were resuspended in DMEM, 1% FBS. HFFs were grown to full confluence and infected with GFP tagged HCMV at the MOIs indicated in the figure legends. HBV-positive sera were used to infect HepG2 cells as previously described (Paran et al., 2001, Bchini et al., 1990, Gripon et al., 1988, Vivekanandan et al., 2010, Zhu et al., 2016) . HepG2 cells were made permissive to HBV virus infection by adding 3% PEG (polyethylglycol) and 0.5% DMSO (dimethylsulphoxide). The cells were infected in 1% FBS containing DMEM, 3% PEG and 0.5% DMSO with the HBV-positive sera. After 6-7 hours, the cells were washed with phosphate-buffered saline (PBS) and then were resuspended in DMEM, 10% FBS, 3% PEG and 0.5% DMSO. For electroporation of human PBMCs, 1 X 10^6 cells were suspended in Opti-MEM (Invitrogen) containing 50 nM mirVana miRNA mimics (Ambion). The cells were pulsed twice with 1000 V for 0.5 ms with a pulse interval of 5 s with the Gene Pulser Xcell electroporation system. The cells were then transferred to RPMI supplemented with 10% FBS (Ingle et al., 2015).

Transfection of cells with miRNA mimics, inhibitors and control mimics/inhibitors and/or plasmids was performed with Lipofectamine 2000 or 3000 (Invitrogen) according to the manufacturer's protocol. Poly IC (Invivogen) was mixed with Lipofectamine 2000 before being used to transfect cells. ssRNA (Invitrogen) were used to stimulate the cells as mentioned in the figure legends. DMEM, FBS, Opti-MEM, RPMI, and Lipofectamine 2000/3000 were purchased from Invitrogen. The miR-30e mimic (miR-30e) (Invitrogen: Catalog number#4464066) or a nonspecific miRNA negative control#1 (miR-NC1) (Invitrogen: Catalog number#4464058) was used according to the manufacturer's instructions (Applied Biosystems). The miR-30e inhibitor (AmiR-30e) (Invitrogen: Catalog number#4464066) was used to inhibit miR-30e expression in transfected cells or a nonspecific Anti-miRNA negative control#1 (Anti-miR-NC1) (Invitrogen: Catalog number#AM17010). The cDNA encoding the 3′-UTR of genes (negative regulators) that were targeted by miR-30e were retrieved from the UCSC gene sorter and was sub-cloned into the pMIR-REPORT luciferase vector. A total of 2.0 kb of sequence upstream of the miR-30e gene was retrieved from the UCSC genome browser. This sequence was amplified by PCR from genomic DNA (source: isolated from A549 cells, using Wizard Genomic DNA isolation kit, Promega: Catalog number#A1120) and was subcloned into the pGL3 basic vector between the KpnI and HindIII sites**.** Plasmids containing Firefly Luciferase gene under *IFNβ, ISRE* and *NFκB* promoters, were obtained from Professor Shizuo Akira's (Osaka University, Japan), *rhIFNβ* (bei resources) and *rhTNFα* (R&D Systems). All sh- clones, were obtained from the whole RNAi human library for shRNA mediating silencing (Sigma, Aldrich) maintained at IISER, Bhopal, India. *In-silico* analysis for miRNA target gene prediction was done as previously described (Ingle et al., 2015).

Quantitative real-time reverse transcription PCR. Total RNA was extracted with the Trizol reagent (Ambion/Invitrogen) and used to synthesize cDNA with the iScript cDNA Synthesis Kit (BioRad, Hercules, CA, USA) according to the manufacturer's protocol. Gene expression was measured by quantitative real-time PCR using gene-specific primers and SYBR Green (Biorad, Hercules, CA, USA) and additionally using 18S and NPM1 (for AGO2-RNA immunoprecipitation experiment) primers for normalization. For quantification of the abundances of miR-30e, real-time PCR analysis was performed with the TaqMan Universal PCR Master Mix (Applied Biosystems) and the miR-30e-5p specific TaqMan miRNA assays. The Taqman U6 assay was used as a reference control. Real time quantification was done using StepOne Plus Real time PCR Systems by Applied BioSystems (Foster City, CA, USA). Primers used for qRT-PCR were listed in Supplementary Table T7.

Luciferase Reporter assays. HEK 293T and HeLa cells (5 X 10^4) were seeded into a 24-well plate and transiently transfected with 25 nM of mimics, 50 ng of the transfection control pRL-TK plasmid (*Renilla* luciferase containing plasmid) and 200 ng of the luciferase reporter plasmid (*Firefly* luciferase containing plasmid) together with/without 300 ng of the various expression plasmids or an empty plasmid as a control according to the respective experiments. The cells were lysed at 24 to 36 hours after transfection and/or infection or stimulations, and finally the luciferase activity in total cell lysates was measured with Glomax (Promega, Madison, WI, USA).

Enzyme-linked immunosorbent assay (ELISA). A549 and HeLa cells were transiently transfected with miR-30e and miR-NC1 and then were infected NDV virus. The culture media were harvested 36 to 40 hours after infection and were analyzed by specific ELISA kits (Becton

Dickinson) according to the manufacturer's instructions to determine the amounts of *IP10* and *IL6* that were secreted by the cells.

RNA immunoprecipitations. RNA immunoprecipitations were performed as described previously (Meister et al., 2004, Beitzinger and Meister, 2011) . The pIRESneo-Flag/HA Ago2 plasmid was a gift from Professor T. Tuschl (Addgene plasmid #10822). Briefly, HEK 293T cells transfected with miRNA and infected with NDV were lysed in 0.5% NP-40, 150 mM KCl, 25 mM tris-glycine (pH 7.5) and incubated with M2 Flag affinity beads (Sigma) overnight. The lysate was then washed with 300 mM NaCl, 50 mM tris-glycine (pH 7.5), 5 mM $MgCl_2$, and 0.05% NP-40. The extraction of RNA from the immunoprecipitated RNPs was performed with the Trizol reagent (Ambion, Invitrogen) according to the manufacturer's protocol.

Fluorescence-activated cell sorting (FACS) Cytometry Analysis. A549 and HeLa cells were grown to 70-80% confluence, then treated with mimics and negative control reagents and finally infected with SeV-RFP and NDV-GFP. After 24 hours of infection, cells were trypsinized, harvested and then washed with PBS thrice and finally resuspended in PBS for FACS analysis as described in figure legends. Human PBMCs were treated with DNA and or camptothecin (0.3μM) to estimate apoptosis levels. At desired time points, cells were analyzed by staining with FITC-labeled Annexin V and propidium iodide (Becton Dickinson, USA) as per manufacturer's instructions and stained cells were analyzed using a FACS Aria III (Becton Dickinson) and data were analyzed by using FlowJo software (FlowJo, Ashland, OR, USA).

Immunoblotting analysis. After cells were transfected with miRNA mimic and controls then after infected with NDV and/or NDV-GFP (as indicated in figures), lysates were collected and subjected to western blotting analysis as previously described (Ingle et al., 2015, Kumar et al., 2015) . Cells were harvested after 36 hours of infection with standard ice-cold cell lysis buffer supplemented with 1 X protease inhibitor cocktail (obtained from Sigma, Aldrich). Immunoblotting were done as previously described (Kumar et al., 2015) . Immunoblotted nitrocellulose membrane was imaged with LI-COR system. Anti–GFP antibody was obtained from Sigma-Aldrich, anti-TRIM38 (from ImmunoTag,), anti-TANK, SOCS3, BECN1 (from Cloud-Clone Corporation), anti-ATG12 (from Cell Signaling Technology), anti-SOCS1 (from Santa Cruz) and anti γ-Tubulin (from Sigma, Aldrich). IR dye labeled anti-Rabbit and anti-Mouse IgG (secondary antibody), were purchased from LI-COR. Densitometry analysis was performed by Image J (Fiji) software.

Microscopy. HeLa cells were transfected with miRNA mimic and infected with NDV-GFP were fixed with 4% PFA for 15 min at room temperature; permeabilized with 0.05% Triton X-100 in 1 x PBS for 10 min at room temperature; blocked with bovine serum albumin (5 mg/ml) in PBS, 0.04% Tween 20 for 30 min and incubated for 1 hour with the relevant primary antibodies diluted in blocking buffer. The cells were then washed three times with PBS and incubated for 1 hour with the appropriate secondary antibodies at room temperature. Nuclei were stained with DAPI, and the cells were then analyzed with an LSM 780 confocal laser microscope (Carl Zeiss). The images were analyzed using ImageJ processing software. HCMV infection (GFP fluorescence) in HFFs miRNA mimic and control mimic transfected cells was visualized with Inverted microscope Vert.A1 (AXIO) by Zeiss.

RNA-Sequencing data analysis. Trizol reagent (Ambion, Invitrogen) was used to isolate total RNA that was processed to prepare cDNA libraries using TruSeq technology according to the manufacturer's instructions protocol (Illumina, San Diego, CA). Libraries were sequenced using Illumina NovaSeq 6000, with a read length of 101 bp, by Bencos Research Solutions Pvt. Ltd., Bangalore, India. FastQC (0.11.5) was used to access the read quality of the raw data. Trimmomatic was used to remove Illumina adaptors and sliding-window approach was used for the quality filtering of reads. Approximately 20 million cleaned pair-end sequencing reads from each sample were uploaded to the Galaxy web platform and were analyzed at https://usegalaxy.org. HISAT2 was used to map the reads with the reference human genome (hg38). StringTie was used to assemble the aligned RNA-Seq reads into transcripts and estimate the abundance of the assembled transcripts. DESeq2 was used for differential expression analysis of genes between groups (Love et al., 2014) . Various R packages were used to visualize the expression and differential expression outcomes. Gene ontology (GO) analysis was done using the web-based Gene Set Analysis toolkit, and analysis of upregulated KEGG pathways was done using Enrichr. Cluster 3.0 and TreeView 1.1.6 were used for making heat maps. All the addressed analysis was demonstrated as described previously (Kumar et al., 2018) .

Statistical analysis. All experiments were carried out along with the appropriate controls, indicated as untreated/untransfected cells (Ctrl) or transfected with the transfection reagent alone (Mock). Experiments were performed in duplicates or triplicates for at least two or three times independently. GraphPad Prism 5.0 (GraphPad Software, La Jolla, CA, USA) was used for statistical analysis. The differences between two groups were compared by using an unpaired two-tailed Student's t-test and/or Mann Whitney test additionally the paired data was analyzed using

paired t-test and/or Wilcoxon sign rank test. While the differences between three groups or more were compared by using analysis of variance (ANOVA) with Tukey test. Differences were considered to be statistically significant when $P < 0.05$. Statistical significance in the figures is indicated as follows: $***P < 0.001$, $**P < 0.01$, $*P < 0.05$; *ns*, not significant.

References

ALIBERTI, J., SCHULZ, O., PENNINGTON, D. J., TSUJIMURA, H., REIS E SOUSA, C., OZATO, K. & SHER, A. 2003. Essential role for ICSBP in the in vivo development of murine CD8alpha + dendritic cells. *Blood,* 101**,** 305-10.

BCHINI, R., CAPEL, F., DAUGUET, C., DUBANCHET, S. & PETIT, M. A. 1990. In vitro infection of human hepatoma (HepG2) cells with hepatitis B virus. *J Virol,* 64**,** 3025-32.

BEITZINGER, M. & MEISTER, G. 2011. Experimental identification of microRNA targets by immunoprecipitation of Argonaute protein complexes. *Methods Mol Biol,* 732**,** 153-67.

GRIPON, P., DIOT, C., THEZE, N., FOUREL, I., LOREAL, O., BRECHOT, C. & GUGUEN-GUILLOUZO, C. 1988. Hepatitis B virus infection of adult human hepatocytes cultured in the presence of dimethyl sulfoxide. *J Virol,* 62**,** 4136-43.

INGLE, H., KUMAR, S., RAUT, A. A., MISHRA, A., KULKARNI, D. D., KAMEYAMA, T., TAKAOKA, A., AKIRA, S. & KUMAR, H. 2015. The microRNA miR-485 targets host and influenza virus transcripts to regulate antiviral immunity and restrict viral replication. *Sci Signal,* 8**,** ra126.

KUMAR, A., KUMAR, A., INGLE, H., KUMAR, S., MISHRA, R., VERMA, M. K., BISWAS, D., KUMAR, N. S., MISHRA, A., RAUT, A. A., TAKAOKA, A. & KUMAR, H. 2018. MicroRNA hsa-miR-324-5p Suppresses H5N1 Virus Replication by Targeting the Viral PB1 and Host CUEDC2. *J Virol,* 92.

KUMAR, S., INGLE, H., MISHRA, S., MAHLA, R. S., KUMAR, A., KAWAI, T., AKIRA, S., TAKAOKA, A., RAUT, A. A. & KUMAR, H. 2015. IPS-1 differentially induces TRAIL, BCL2, BIRC3 and PRKCE in type I interferons-dependent and -independent anticancer activity. *Cell Death Dis,* 6**,** e1758.

LOVE, M. I., HUBER, W. & ANDERS, S. 2014. Moderated estimation of fold change and dispersion for RNA-seq data with DESeq2. *Genome Biol,* 15**,** 550.

MEISTER, G., LANDTHALER, M., PATKANIOWSKA, A., DORSETT, Y., TENG, G. & TUSCHL, T. 2004. Human Argonaute2 mediates RNA cleavage targeted by miRNAs and siRNAs. *Mol Cell,* 15**,** 185-97.

PARAN, N., GEIGER, B. & SHAUL, Y. 2001. HBV infection of cell culture: evidence for multivalent and cooperative attachment. *EMBO J,* 20**,** 4443-53.

SATO, S., LI, K., KAMEYAMA, T., HAYASHI, T., ISHIDA, Y., MURAKAMI, S., WATANABE, T., IIJIMA, S., SAKURAI, Y., WATASHI, K., TSUTSUMI, S., SATO, Y., AKITA, H., WAKITA, T., RICE, C. M., HARASHIMA, H., KOHARA, M., TANAKA, Y. & TAKAOKA, A. 2015. The RNA sensor RIG-I dually functions as an innate sensor and direct antiviral factor for hepatitis B virus. *Immunity,* 42**,** 123-32.

TAMURA, T., TAILOR, P., YAMAOKA, K., KONG, H. J., TSUJIMURA, H., O'SHEA, J. J., SINGH, H. & OZATO, K. 2005. IFN regulatory factor-4 and -8 govern dendritic cell subset development and their functional diversity. *J Immunol,* 174**,** 2573-81.

VIVEKANANDAN, P., DANIEL, H. D., KANNANGAI, R., MARTINEZ-MURILLO, F. & TORBENSON, M. 2010. Hepatitis B virus replication induces methylation of both host and viral DNA. *J Virol,* 84**,** 4321-9.

ZHU, X., XIE, C., LI, Y. M., HUANG, Z. L., ZHAO, Q. Y., HU, Z. X., WANG, P. P., GU, Y. R., GAO, Z. L. & PENG, L. 2016. TMEM2 inhibits hepatitis B virus infection in HepG2 and HepG2.2.15 cells by activating the JAK-STAT signaling pathway. *Cell Death Dis,* 7**,** e2239.